

















































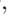



## Searching for Exotrojans in Pulsar Systems

JACKSON D. TAYLOR <sup>1,2</sup> EMMANUEL FONSECA <sup>1,2</sup> LANKESWAR DEY <sup>1,2</sup> SERGEY ZHARIKOV <sup>3</sup>  
AIDA KIRICHENKO <sup>3</sup> JOSEPH GLASER <sup>1,2</sup> GABRIELLA AGAZIE <sup>4</sup> AKASH ANUMARLAPUDI <sup>5</sup>  
ANNE M. ARCHIBALD <sup>6</sup> ZAVEN ARZOUMANIAN <sup>7</sup> PAUL T. BAKER <sup>8</sup> PAUL R. BROOK <sup>9</sup>  
H. THANKFUL CROMARTIE <sup>10</sup> KATHRYN CROWTER <sup>11</sup> MEGAN E. DECESAR <sup>12,\*</sup> PAUL B. DEMOREST <sup>13</sup>  
TIMOTHY DOLCH <sup>14,15</sup> ELIZABETH C. FERRARA <sup>16,17,18</sup> WILLIAM FIORE <sup>11</sup> GABRIEL E. FREEDMAN <sup>18</sup>  
NATE GARVER-DANIELS <sup>1,2</sup> PETER A. GENTILE <sup>1,2</sup> DEBORAH C. GOOD <sup>19</sup> JEFFREY S. HAZBOUN <sup>20</sup>  
ROSS J. JENNINGS <sup>1,2,†</sup> MEGAN L. JONES <sup>4</sup> DAVID L. KAPLAN <sup>4</sup> MATTHEW KERR <sup>21</sup> MICHAEL T. LAM <sup>22,23,24</sup>  
T. JOSEPH W. LAZIO<sup>25</sup> DUNCAN R. LORIMER <sup>1,2</sup> JING LUO <sup>26,‡</sup> RYAN S. LYNCH <sup>27</sup> ALEXANDER MCEWEN <sup>4</sup>  
MAURA A. MCLAUGHLIN <sup>1,2</sup> NATASHA MCMANN <sup>28</sup> BRADLEY W. MEYERS <sup>29,30</sup> CHERRY NG <sup>31</sup>  
DAVID J. NICE <sup>32</sup> TIMOTHY T. PENNUCCI <sup>33</sup> BENETGE B. P. PERERA <sup>34</sup> NIHAN S. POL <sup>35</sup>  
HENRI A. RADOVAN <sup>36</sup> SCOTT M. RANSOM <sup>37</sup> PAUL S. RAY <sup>21</sup> ANN SCHMIEDEKAMP <sup>38</sup> CARL SCHMIEDEKAMP <sup>38</sup>  
BRENT J. SHAPIRO-ALBERT <sup>1,2,39</sup> INGRID H. STAIRS <sup>11</sup> KEVIN STOVALL <sup>13</sup> ABHIMANYU SUSOBHANAN <sup>40</sup>  
JOSEPH K. SWIGGUM <sup>32,†</sup> AND HALEY M. WAHL <sup>1,2</sup>

<sup>1</sup>Department of Physics and Astronomy, West Virginia University, P.O. Box 6315, Morgantown, WV 26506, USA

<sup>2</sup>Center for Gravitational Waves and Cosmology, West Virginia University, Chestnut Ridge Research Building, Morgantown, WV 26505, USA

<sup>3</sup>Instituto de Astronomía, Universidad Nacional Autónoma de México, Apdo. Postal 877, Ensenada, Baja California 22800, México

<sup>4</sup>Center for Gravitation, Cosmology and Astrophysics, Department of Physics and Astronomy, University of Wisconsin-Milwaukee, P.O. Box 413, Milwaukee, WI 53201, USA

<sup>5</sup>Department of Physics and Astronomy, University of North Carolina, Chapel Hill, NC 27599, USA

<sup>6</sup>Newcastle University, NE1 7RU, UK

<sup>7</sup>X-Ray Astrophysics Laboratory, NASA Goddard Space Flight Center, Code 662, Greenbelt, MD 20771, USA

<sup>8</sup>Department of Physics and Astronomy, Widener University, One University Place, Chester, PA 19013, USA

<sup>9</sup>Institute for Gravitational Wave Astronomy and School of Physics and Astronomy, University of Birmingham, Edgbaston, Birmingham B15 2TT, UK

<sup>10</sup>National Research Council Research Associate, National Academy of Sciences, Washington, DC 20001, USA resident at Naval Research Laboratory, Washington, DC 20375, USA

<sup>11</sup>Department of Physics and Astronomy, University of British Columbia, 6224 Agricultural Road, Vancouver, BC V6T 1Z1, Canada

<sup>12</sup>Department of Physics and Astronomy, George Mason University, Fairfax, VA 22030, resident at the U.S. Naval Research Laboratory, Washington, DC 20375, USA

<sup>13</sup>National Radio Astronomy Observatory, 1003 Lopezville Rd., Socorro, NM 87801, USA

<sup>14</sup>Department of Physics, Hillsdale College, 33 E. College Street, Hillsdale, MI 49242, USA

<sup>15</sup>Eureka Scientific, 2452 Delmer Street, Suite 100, Oakland, CA 94602-3017, USA

<sup>16</sup>Department of Astronomy, University of Maryland, College Park, MD 20742, USA

<sup>17</sup>Center for Research and Exploration in Space Science and Technology, NASA/GSFC, Greenbelt, MD 20771

<sup>18</sup>NASA Goddard Space Flight Center, Greenbelt, MD 20771, USA

<sup>19</sup>Department of Physics and Astronomy, University of Montana, 32 Campus Drive, Missoula, MT 59812

<sup>20</sup>Department of Physics, Oregon State University, Corvallis, OR 97331, USA

<sup>21</sup>Space Science Division, Naval Research Laboratory, Washington, DC 20375-5352, USA

<sup>22</sup>SETI Institute, 339 N Bernardo Ave Suite 200, Mountain View, CA 94043, USA

<sup>23</sup>School of Physics and Astronomy, Rochester Institute of Technology, Rochester, NY 14623, USA

<sup>24</sup>Laboratory for Multiwavelength Astrophysics, Rochester Institute of Technology, Rochester, NY 14623, USA

<sup>25</sup>Independent Researcher

<sup>26</sup>Department of Astronomy & Astrophysics, University of Toronto, 50 Saint George Street, Toronto, ON M5S 3H4, Canada

<sup>27</sup>Green Bank Observatory, P.O. Box 2, Green Bank, WV 24944, USA

<sup>28</sup>Department of Physics and Astronomy, Vanderbilt University, 2301 Vanderbilt Place, Nashville, TN 37235, USA

<sup>29</sup>Australian SKA Regional Centre (AusSRC), Curtin University, Bentley, WA 6102, Australia

<sup>30</sup>International Centre for Radio Astronomy Research (ICRAR), Curtin University, Bentley, WA 6102, Australia

Corresponding author: Jackson D. Taylor

jdt00012@mix.wvu.edu, jacksondtaylor4@gmail.com

<sup>31</sup>*Dunlap Institute for Astronomy and Astrophysics, University of Toronto, 50 St. George St., Toronto, ON M5S 3H4, Canada*

<sup>32</sup>*Department of Physics, Lafayette College, Easton, PA 18042, USA*

<sup>33</sup>*Institute of Physics and Astronomy, Eötvös Loránd University, Pázmány P. s. 1/A, 1117 Budapest, Hungary*

<sup>34</sup>*Arecibo Observatory, HC3 Box 53995, Arecibo, PR 00612, USA*

<sup>35</sup>*Department of Physics, Texas Tech University, Box 41051, Lubbock, TX 79409, USA*

<sup>36</sup>*Department of Physics, University of Puerto Rico, Mayagüez, PR 00681, USA*

<sup>37</sup>*National Radio Astronomy Observatory, 520 Edgemont Road, Charlottesville, VA 22903, USA*

<sup>38</sup>*Department of Physics, Penn State Abington, Abington, PA 19001, USA*

<sup>39</sup>*Giant Army, 915A 17th Ave, Seattle WA 98122*

<sup>40</sup>*Max-Planck-Institut für Gravitationsphysik (Albert-Einstein-Institut), Callinstraße 38, D-30167 Hannover, Germany  
Leibniz Universität Hannover, D-30167 Hannover, Germany*

## ABSTRACT

Trojan asteroids are found in the equilateral triangle Lagrange points of the Sun-Jupiter system in great number, though they also exist less prolifically in other parts of the Solar System. Despite up to planetary mass Trojans being predicted in extrasolar systems (i.e. exotrojans), they remain unconfirmed, although strong candidate evidence has emerged recently. For the first time, we extend the search for exotrojans to radio pulsars with low-mass ( $\sim 0.01 M_{\odot}$ ) companions using accurately measured pulse times of arrival. With techniques developed for detecting the reflex motion of a star due to a librating Trojan, we place  $\sim 1 M_{\oplus}$  upper mass constraints on potential exotrojans around eight pulsars observed in the NANOGrav 15-year data set. We find weak evidence consistent with  $\sim 2\text{--}4 M_{\text{J}}$  exotrojans in the PSR J0023+0923 and PSR J1705–1903 binary systems, though the signals likely have a different, unknown source. We also place a libration-independent upper mass constraint of  $\sim 8 M_{\text{J}}$  on exotrojans in the PSR J1641+8049 system by looking for an inconsistency between the times of superior conjunction as measured by optical light curves and those predicted by radio timing. These results offer initial observational constraints on the existence of exotrojans around pulsars, while their possible formation mechanisms remain unexplored.

*Keywords:* Pulsar planets (1304), Trojan planets (1716), Millisecond pulsars (1062)

## 1. INTRODUCTION

Trojans are objects that reside in the  $L_4$  or  $L_5$  Lagrange points of two massive bodies. In our case, the relevant configuration consists of a pulsar, its low-mass companion (which we call the secondary), and a possible Trojan. The Trojan shares the secondary’s mean motion and trails or leads the secondary by  $60^\circ$  throughout its orbit. In the Jupiter-Sun system alone, there are over ten thousand confirmed Trojans (e.g., J. Li et al. 2023) along with estimates of hundreds of thousands more that have diameters above  $\sim 2$  km (see, e.g., D. C. Jewitt et al. 2000; F. Yoshida & T. Nakamura 2005). Every Solar System planet currently has Trojans of its own, barring Mercury—which may lack confirmed Trojans due to observational difficulties—and there are even Trojans of the Saturn-Tethys system.

The abundance of Trojans in our Solar System suggests that extrasolar Trojans (exotrojans) should also be common. Indeed, any robust Solar System formation theory must allow for their creation, and many of these theories do not just predict Trojan asteroids but also, surprisingly, Trojans of planetary mass (e.g., G. Laughlin & J. E. Chambers 2002; P. Cresswell & R. P. Nelson 2008; W. Lyra et al. 2009; M. Montesinos et al. 2020). Once formed, it has been shown that these Trojans can find themselves in relatively large stable regions (J. M. A. Danby 1964; C. Giuppone et al. 2010; A. Leleu et al. 2015). In the case of circular orbits, the triangular Lagrange points are only stable if

$$\frac{m_{\text{p}}m_{\text{c}} + m_{\text{p}}m_{\text{T}} + m_{\text{c}}m_{\text{T}}}{(m_{\text{p}} + m_{\text{c}} + m_{\text{T}})^2} < \frac{1}{27}, \quad (1)$$

where  $m_{\text{p}}$  is the mass of the host star (a pulsar in this study),  $m_{\text{c}}$  is the mass of the secondary (the pulsar’s dominant companion), and  $m_{\text{T}}$  is the mass of the Trojan (the pulsar’s lowest mass companion; M. Gascheau 1843). J. M. A. Danby (1964) showed that introducing

\* Resident at the Naval Research Laboratory

† NANOGrav Physics Frontiers Center Postdoctoral Fellow

‡ Deceased

a non-zero orbital eccentricity generally decreases the window of stable masses.

Unless the Trojan is librating around its stable point, the measured gravitational effects on the star from a single orbiting companion are degenerate with those of two co-orbiting companions up to  $\mathcal{O}(e_o^2)$  (A. Leleu et al. 2017), where  $e_o$  is the orbital eccentricity. This degeneracy helps explain why, despite their prevalence in our Solar System and their accompanying formation models, no Trojans outside the Solar System have yet been confirmed. E. B. Ford & B. S. Gaudi (2006) showed that combining radial velocity data with transit-timing data breaks this degeneracy. A. Leleu et al. (2017) further formalized their approach into the robust  $\alpha$ -test method to include the results of several transits. O. Balsalobre-Ruza et al. (2024) applied this technique to identify one of the strongest candidates to date with a  $3\text{-}\sigma$  detection, building on the earlier works of J. Lillo-Box et al. (2018a,b). These works are part of, or helped form the foundation for, the broader TROY project,<sup>41</sup> which seeks to discover the first extrasolar Trojan planets. While most of their work has been confined to optical observations of main-sequence stars, O. Balsalobre-Ruza et al. (2023) potentially identified an accumulation of gas and dust that might be a forming Trojan in the PDS 70 protoplanetary disk (e.g., M. Keppler et al. 2018; S. Haffert et al. 2019).

Other studies have searched for photometric transits of the Trojans themselves. M. Janson (2013) used the *Kepler* space telescope to rule out transiting Trojans down to  $1 R_{\oplus}$  in 2244 systems, and R. Moldovan et al. (2010) used the *MOST* satellite to place a lunar mass upper limit on a Trojan in the HD 209458 system. Rather than looking for transits from individual Trojans, M. Hippke & D. Angerhausen (2015) looked for a cumulative Trojan effect across nearly 4000 planets by adding their *Kepler* light curves coherently by orbital phase, and identified potential transits of the stacked light curves at the expected  $L_4$  and  $L_5$  orbital phases. The main problem with identifying Trojans transiting their host stars is the fact that we expect exotrojans to have a broad range of orbital inclinations, as is the case for the Jupiter Trojans (F. Yoshida & T. Nakamura 2005; D. Nesvorný et al. 2013; W. F. Bottke et al. 2023). Therefore, the dominant *Kepler* planet transiting its host star does not guarantee that any Trojan planets will also transit during any given observation. In contrast, the  $\alpha$ -test method does not rely on in-plane Trojans.

While almost every exotrojan search has been done around main-sequence stars, as detailed above, no study has looked for them around pulsar binary systems. Just as we expect Trojans to form around ordinary stars during the protoplanetary disk phase (e.g., M. Montesinos et al. 2020), Trojans may also form around pulsars when a disk is present and then settle via gas drag (W. Lyra et al. 2009) into stable so-called tadpole (T-type) orbits. Such a disk can form in at least two possible ways. One type of pulsar disk, the supernova fallback disk, forms when some of the material from the supernova that formed the pulsar returns to the pulsar and collapses into a disk (E. A. Behrens et al. 2020; K. Xu et al. 2024). Such disks are a plausible formation channel for pulsar planets (D. Lin et al. 1991; A. Wolszczan & D. A. Frail 1992), and would explain why the planets around PSR B1257+12 have similar inclinations (M. Konacki & A. Wolszczan 2003).

The other possible type of pulsar disk forms when the compact pulsar in a binary system strips material from its evolving, ablated companion. This material forms an accretion disk, which collects onto the pulsar and transitions the pulsar into a millisecond pulsar (MSP) (A. M. Archibald et al. 2009; A. Papitto & D. d. Martino 2021). Before the accretion disk dissipates, it may form planets (A. Patruno & M. Kama 2017; E. A. Behrens et al. 2020), an asteroid belt (R. Shannon et al. 2013), or Trojan planets in 1:1 resonance with the pulsar’s companion, as in the case of protoplanetary-disk-formed Trojans (W. Lyra et al. 2009; M. Montesinos et al. 2020). Potential Trojans, too, may be stripped of their material, but the timescale of complete dissipation is unclear, with some estimates ranging up to a few Gyr for the secondary (e.g. S. Ginzburg & E. Quataert 2020). This picture is complicated by the fact that material from the secondary could continue to fall into the Triangular Lagrange points. In any case, detecting an interloping Trojan may be possible even if it lasts just a few hundred Myr before complete dissipation.

The above pulsar Trojan formation discussion lays out plausible channels, but the possible existence of pulsar Trojans remains speculative. Future theoretical work is required to draw definitive connections between protoplanetary disks and pulsar-centered disks with respect to Trojan creation. Although the existence of pulsar Trojans is uncertain, the history of serendipitous astronomical discoveries in the last several decades—including pulsars, fast radio bursts, and hot Jupiters—motivates their search. In any case, our results provide an independent observational baseline for future theoretical studies, such as hydrodynamical simulations, of pulsar Trojan viability.

<sup>41</sup> [www.troy-project.com](http://www.troy-project.com)

The first exoplanet was discovered around a pulsar (A. Wolszczan & D. A. Frail 1992), and ever since there has been a growing interest in discovering massive bodies in the environs of pulsars. Besides studies looking for planets in the ordinary P-type orbit (e.g., M. Bailes et al. 2011; R. Spiewak et al. 2018; E. A. Behrens et al. 2020; I. C. Nițu et al. 2022), pulsar asteroid belts (R. Shannon et al. 2013; R. J. Jennings et al. 2020a) and freely-floating planets gravitationally scattering with pulsars (R. J. Jennings et al. 2020b; L. Dey et al. 2026) have also been investigated. In this work, we turn the search to Trojans that may reside in black widow pulsar systems—binaries characterized by an MSP with a low-mass ( $\sim 0.01 M_{\odot}$ ) companion (e.g., T. Shahbaz et al. 2017)—and are therefore likely to follow the stability criterion given in Equation 1.

To conduct the first-ever search for Trojan planets in pulsar binary systems, we use the North American Nanohertz Observatory for Gravitational Waves (NANOGrav) 15-year (NG15yr) narrow-band dataset (G. Agazie et al. 2023) as well as optical-band light curves of PSR J1641+8049 from A. Y. Kirichenko et al. (2024) to search for pulsar systems bearing Trojans in the T-type configuration. We ignore horseshoe configurations because these systems do not yield a closed-form waveform in the pulse times of arrival (TOAs; see Section 2.2 and A. Leleu et al. 2015). A Trojan in the T-type configuration librates around a particular triangular Lagrange point, while a Trojan in the horseshoe configuration will repeatedly librate between  $L_4$  and  $L_5$  going through  $L_3$ . Excluding horseshoe orbiters does not greatly limit our search, as not only are they less common in the Solar System (e.g., M. Kaplan & S. Cengiz 2020), but also their stability criterion are stricter (e.g., G. Laughlin & J. E. Chambers 2002).

We outline our methods in Section 2, select our observed data in Section 3, display and discuss our results in Section 4, and conclude with a broader discussion in Section 5.

## 2. METHODS

A. Leleu et al. (2015, 2017) showed that the signal observed from a star-exoplanet-exotrojan system is largely degenerate with that from an ordinary star-exoplanet system. This is due to the secondary and Trojan forming a combined effective companion. The TOAs will indicate the pulsar and a combined effective companion are orbiting a center of mass. The following subsections discuss two ways to break this degeneracy in the context of pulsar binary systems.

The first method uses both optical light curves and radio pulsar TOAs. Both the light curves and TOAs can

independently measure the time of superior conjunction (TSC), which is when the pulsar’s companion is furthest from the Earth in its orbit. A discrepancy between the light-curve-measured TSC and TOA-measured TSC can reveal the presence of a mass accumulation along the orbit in the system. This is an adaptation the method developed by E. B. Ford & B. S. Gaudi (2006) for exoplanets orbiting main-sequence stars. In their case, they compare the transiting time of the secondary measured from photometry—in other words, the time of inferior conjunction (TIC)—with the estimated transiting time from radial velocities. The orbital planes of the secondaries in our study are not “edge-on” with respect to our LOS, so we cannot measure their direct transits. However, we can measure their TSCs which corresponds to peak optical flux, as the secondaries are tidally locked with pulsar. Note that we assume negligible flux contributions from the pulsar and any Trojans. Analogously to radial velocities, TOAs trace the Keplerian orbit from the effective orbiting mass (secondary-exotrojan) by measuring the pulsar LOS position. Therefore, the TOAs uniquely determine the relevant Keplerian parameters (e.g., J. Taylor et al. 2024), which give the TSC. See Section 2.1 for more details and Figures 1A and 1C of E. B. Ford & B. S. Gaudi 2006 for an illustration of the concept.

The second method requires only TOAs, but only works if any Trojan and secondary in the system is librating around the stable Lagrange point. If the Trojan and secondary are librating with some frequency, the effective companion-pulsar center of mass will also oscillate at the same frequency. A pulsar orbiting an oscillating center of mass no longer produces TOAs degenerate with those of a two-body system, and allows us to measure important properties and masses of the system. This method comes directly from A. Leleu et al. (2015), where they derive both the line-of-sight position and radial velocity of a main-sequence star that hosts librating co-orbitals. As mentioned above, we can use the TOAs to measure the pulsar’s line-of-sight (LOS) position. We expand upon their LOS position derivation in Appendix A, including a minor algebraic correction. This libration-dependent method can be used to detect a single Trojan in a pulsar binary system. In the case of a Trojan swarm, this method remains effective in detecting the highest-mass Trojan, provided this Trojan is massive enough to allow gravitational effects from the other Trojans to be ignored. See Section 2.2 for more details.

In this work, we quote posterior medians with uncertainties enclosing the 68% credible interval. We quote our upper limits at 95% credibility. We use both the

parentheses-on-the-last-digit(s) convention and the  $\pm$  notation to express these 68% uncertainties. Throughout,  $\log$  denotes the base-10 logarithm.

### 2.1. Conjunction Inconsistency

Let  $T_{o,s}$  and  $T_{o,i}$  be the times of superior and inferior conjunction, respectively, as measured through optical band data, and let  $T_{r,s}$  and  $T_{r,i}$  be the same as measured by the TOA-determined pulsar reflex motion. Given how C. Lange et al. (2001) define  $T_{asc}$ , radio pulsar timing predicts superior and inferior conjunctions to occur at  $T_{r,s} = T_{asc} - P_b/4$  and  $T_{r,i} = T_{asc} + P_b/4$ , respectively, where we ignore orbital eccentricity ( $e_o$ ) effects.  $P_b$  is the binary orbital period and  $T_{asc}$  is the time of the ascending node as defined in C. Lange et al. (2001). We ignore  $\mathcal{O}(e_o)$  effects throughout this study, because the highest orbital eccentricity of the pulsars studied is of the order  $10^{-4}$ . E. B. Ford & B. S. Gaudi (2006) show that any discrepancy in  $T_{o,s}$  and  $T_{r,s}$  (or  $T_{o,i}$  and  $T_{r,i}$ ) could indicate the presence of an exotrojan with the time difference directly mapped from the exotrojan mass:

$$\Delta t \approx \pm 35.6 \left( \frac{P_b}{3 \text{ h}} \right) \left( \frac{0.04 M_\odot}{m_T + m_c} \right) \left( \frac{\Delta m_T}{1 M_J} \right) \text{ s}, \quad (2)$$

where  $\Delta t = T_{o,s} - T_{r,s}$  and  $\Delta m_T$  is the mass difference between the  $L_4$  and  $L_5$  Lagrange points. Here, again, we ignore the  $\mathcal{O}(e_o)$  term. Therefore, Trojans present in both points will partially cancel their measurable effects. We use this method to rule out a high-mass Trojan in the PSR J1641+8049 system (see Section 4.1) by incorporating its superior conjunction measurements (Section 3.1). We note that this method is inclination independent due to the orbital period and the time delay both being inclination independent.

#### 2.1.1. Determination of the Times of Optical Superior Conjunction

Some binary pulsar optical light curves show a clearly periodic structure with a period equal to the binary period (e.g., Figure 4 of A. Y. Kirichenko et al. 2024), explained by the neutron star heating its tidally locked companion. Therefore, assuming the symmetric heating models of S. Zharikov et al. (2013, 2019) and neglecting the heating of the Trojan, the peak flux corresponds to the time(s) of superior conjunction of the secondary.

To derive the times of the superior conjunction and their associated uncertainties, we analyzed light curve data of the PSR J1641+8049 system. We show the optical light curve in Figure 1. More details can be found in Section 3.1 and D. Mata Sánchez et al. (2023); A. Y. Kirichenko et al. (2024). We adopt the emission

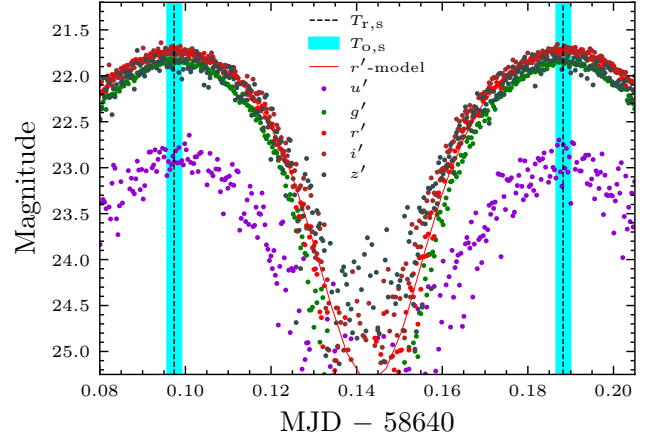


**Figure 1.** High PERFORMANCE CAMERA light curve data from the 10.4m Gran Telescopio Canarias of the PSR J1641+8049 system for each Sloan band. The data was first presented in D. Mata Sánchez et al. (2023). We show the best-fit model for the  $r'$  band as an example, with the remaining model curves shown in A. Y. Kirichenko et al. (2024). Every band except  $u'$  was used in calculating  $T_{o,s}$ . The vertical dashed line marks the TSC as predicted by radio timing. The uncertainty on the TOA-predicted TSC is far smaller than the  $\hat{x}$ -axis scale of the figure. The vertical cyan band encloses the 68% confidence interval of the TSC as calculated from the optical light curve.

model of S. Zharikov et al. (2013, 2019) and start with the best-fit parameters found in A. Y. Kirichenko et al. (2024). The emission model assumes symmetric heating with hottest side facing the pulsar. The heating model parameters are the distance from the system to the Earth, the reddening  $E(B - V)$ , the pulsar mass, the companion-to-pulsar mass ratio, the orbital inclination, the Roche lobe filling factor, the effective radiation factor, the companion dark-side temperature, and the time of superior conjunction. For more details on these parameters and the model, see S. Zharikov et al. (2013, 2019); A. Y. Kirichenko et al. (2024) and references therein. We define  $\mathbf{p}$  as the vector of all these parameters, excluding the time of superior conjunction.

Let  $\phi_{\max}$  be the binary phase corresponding to peak light, which is used to calculate the time of superior conjunction. Let  $\phi'_{\max}$  and  $\mathbf{p}'$  be the values of  $\phi_{\max}$  and  $\mathbf{p}$ , respectively, that minimize  $\chi^2$ . While fixing  $\mathbf{p}$  to  $\mathbf{p}'$ , we shift  $\phi_{\max}$  from  $\phi'_{\max}$  and compute the  $\Delta\chi^2$  for each shift,  $\Delta\chi^2(\phi_{\max})$ . The resulting  $\Delta\chi^2$  values form a distribution,  $f(\Delta\chi^2)$ . The 68% uncertainty on  $\phi_{\max}$ ,  $\sigma_{\phi_{\max}}$ , is such that

$$\int_0^{\Delta\chi^2(\sigma_{\phi_{\max}})} f(\Delta\chi^2) d\Delta\chi^2 = 0.68. \quad (3)$$

## 2.2. Librations

A. Leleu et al. (2015) adapted the work of P. Robutel et al. (2011) to determine how a host star’s position (or velocity if spectral data is available) relative to the Solar System barycenter (SSB) will change when a companion and Trojan are present. A pulsar moving relative to the SSB will cause changing light travel time delays, known as Rømer delays, in the pulse TOAs. R. J. Jennings et al. (2020b), for example, showed these delays to be

$$\Delta\tau = -\frac{\mathbf{r}_p \cdot \hat{\mathbf{n}}}{c} \quad (4)$$

when ignoring terms that are degenerate with the pulsar’s pulse period and pulse period time derivative.  $\mathbf{r}_p$  is the pulsar’s position with respect to the system center of mass,  $\hat{\mathbf{n}}$  is the unit vector pointing from the pulsar system barycenter to the SSB, and  $c$  is the speed of light in a vacuum. Therefore,  $\hat{\mathbf{n}}$  is antiparallel to the LOS.

We will now begin the derivation of  $\Delta\tau$  in the case of a librating Trojan in the orbit around a pulsar, but reserve most of the details to Appendix A. Let  $\lambda_T$  and  $\lambda_c$  be the orbital longitudes of the Trojan and secondary, respectively. Let  $\lambda$  be the mass-averaged longitude of the co-orbitals which follows the mean motion and is unaffected by librations. We call the difference in longitude between the co-orbitals the libration angle,  $\zeta$ . The TOAs will indicate the presence of an orbiting combined effective companion, which has longitude  $\phi$ .  $\lambda$  and  $\phi$  are nearly but not exactly identical, with

$$|\phi - \lambda| \lesssim 0.02 \quad (5)$$

shown in Appendix A. Both  $\lambda$  and  $\phi$  evolve over time as the co-orbitals orbit the pulsar according to

$$\lambda = n_b \tilde{t} + \lambda_0, \quad (6)$$

$$\phi = n_b \tilde{t} + \phi_0, \quad (7)$$

where  $n_b = 2\pi/P_b$  is the orbital mean motion,  $\tilde{t}$  is time with respect to the time of the ascending node,  $T_{\text{asc}}$ , and  $\lambda_0$  and  $\phi_0$  are to-be-determined constants. We show in Appendix A that the mass of the fictitious effective companion

$$m_f = (m_c + m_T) \sqrt{1 - \delta(1 - \delta)} + \mathcal{O}\left(\frac{m_T}{m_p}, \frac{m_c}{m_p}\right). \quad (8)$$

Defining

$$\delta = m_c / (m_c + m_T), \quad (9)$$

the mass of the secondary relative to both co-orbitals, the angles of the Trojan and secondary longitudes with respect to  $\lambda$  are  $\delta\zeta$  and  $(1 - \delta)\zeta$ , respectively. P. Robutel

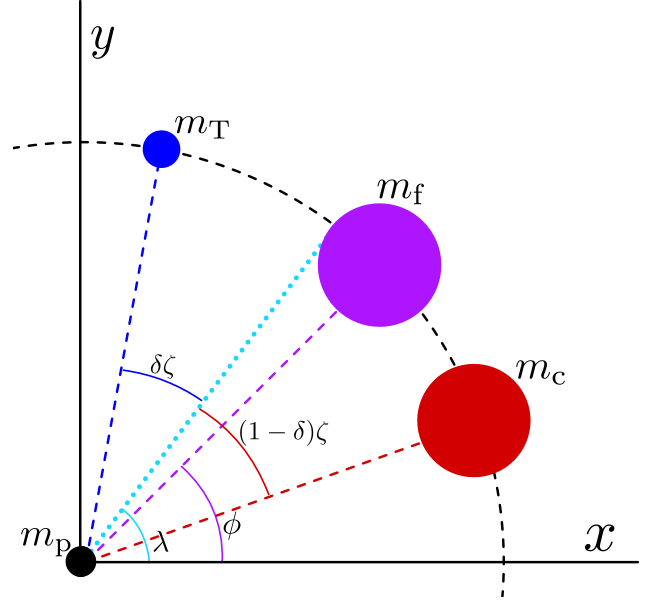


**Figure 2.** The relevant angles in the triangular three-body system.  $m_f$  indicates the fictitious companion, with mass given by Equation 8. The Trojan and companion are shown orbiting counterclockwise here, meaning the Trojan is in the  $L_4$  Lagrange point. See the text for more details. Inspired by Figure 1 of A. Leleu et al. (2015).

et al. (2011) showed that

$$\lambda_T = \lambda + \delta\zeta, \quad (10)$$

$$\lambda_c = \lambda - (1 - \delta)\zeta. \quad (11)$$

Let the plane of the orbit define the  $\hat{x}\hat{y}$ -plane. Without a loss of generality, we place the Earth in the  $\hat{x}\hat{z}$ -plane and define the  $\hat{x}$ -axis to be the projection of the LOS onto the orbital plane. Therefore, the orbital inclination with respect to the plane of the sky,  $I$ , is the angle between the LOS and the  $\hat{z}$ -axis. We define the  $\hat{y}$ -axis such that the  $T_{\text{asc}}$  is the time at which the fictitious companion crosses the negative  $\hat{y}$ -axis. See Figure 2 for a helpful illustration.

When librations are absent,  $\zeta = \pi/3$  for all time. However, in the presence of small librations,  $\zeta$  will oscillate around  $\pi/3$  with (angular) frequency  $\nu$  and amplitude  $z$  (e.g., A. Leleu et al. 2015); i.e.

$$\zeta = z \cos(\nu\tilde{t} + \varphi) + \frac{\pi}{3}, \quad (12)$$

where  $\varphi$  is the vibrational phase at  $t = T_{\text{asc}}$ .  $z$  can vary across otherwise identical systems and is a function of the Trojan’s detailed formation history. We note that  $z$  can be lowered through any sort of dissipative process, such as gas drag (W. Lyra et al. 2009). In contrast,  $\nu$  depends on the masses of the pulsar and co-orbitals.

Namely, [A. Leleu et al. \(2015\)](#) showed that in the low  $\mu$  limit,

$$\nu = n_b \sqrt{\frac{27\mu}{4}}, \quad (13)$$

where

$$\mu = \frac{m_T + m_c}{m_p + m_c + m_T}. \quad (14)$$

However, in the low- $m_T$ -only limit

$$\nu = \frac{n_b}{2} \left[ 2 - \sqrt{27\kappa^2 - 23} \right]^{1/2}, \quad (15)$$

where  $\kappa = (m_p - m_c)/(m_p + m_c)$  ([N. J. Cornish 2001](#); [B. Érdi et al. 2007](#)). Equation 15 is more appropriate than Equation 13 when  $m_T$  is negligible but  $m_c$  is not. There is another frequency associated with librations as well ([B. Érdi et al. 2007](#)), which would add in sum to Equation 12, but [M. Janson \(2013\)](#) showed that its corresponding libration amplitude is much smaller than  $z$ , and therefore can be safely ignored when these systems are on the threshold of detectability.

If  $z = 0$ , then the TOAs are completely degenerate from TOAs from a two-body system. A non-zero  $z$  breaks this degeneracy. The TOA signal, through Equation 4, will have a term degenerate with a two-body system plus a term due to librations. This “libration term” will depend on the mass-averaged semi-major axis of the co-orbitals in the pulsar-centric frame ( $a$ ),  $z$ ,  $\nu$ ,  $n_b$ ,  $I$ , and  $\mu$ . After removing the degenerate two-body term, we derive in Appendix A

$$\Delta\tau = \frac{\mu a \sin I}{c} z \delta (1 - \delta) \left[ \cos(\nu \tilde{t} + \varphi) \cos(n_b \tilde{t} + \theta) + \frac{2}{3} \frac{\nu}{n_b} \sin(\nu \tilde{t} + \varphi) \sin(n_b \tilde{t} + \theta) \right], \quad (16)$$

where

$$\theta = \arctan\left(\frac{\delta\sqrt{3}}{2 - \delta}\right) + \frac{\pi}{3}. \quad (17)$$

In searching for a Trojan in a particular system, see Section 2.2.1, we wish to remove covariances and degeneracies in the prefactor of Equation 16, so we define what we call the libration strength

$$\mathcal{T} = \alpha z \delta (1 - \delta), \quad (18)$$

where

$$\alpha = \frac{\mu a}{c} \sin(I). \quad (19)$$

Therefore, we have

$$\Delta\tau = \mathcal{T} \left[ \cos(\nu \tilde{t} + \varphi) \cos(n_b \tilde{t} + \theta) + \frac{2}{3} \frac{\nu}{n_b} \sin(\nu \tilde{t} + \varphi) \sin(n_b \tilde{t} + \theta) \right]. \quad (20)$$

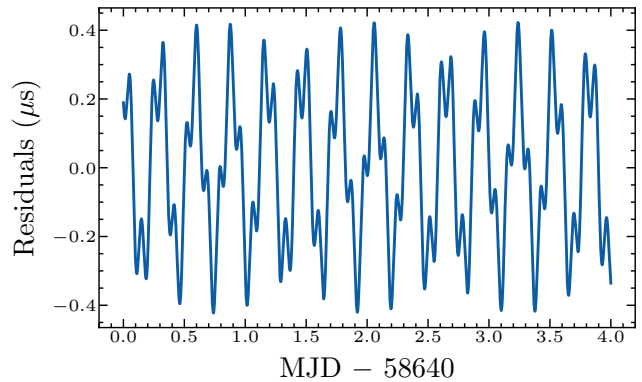


**Figure 3.** Model for the effect of a librating Trojan on the TOA delays (residuals) of PSR J0023+0923. In this example, we set  $m_T = 6 M_J$ ,  $m_p = 1.4 M_\odot$ ,  $m_c = 46 M_J$ ,  $I = 14^\circ$ ,  $z = 0.0001^\circ$ ,  $\varphi = 1.2$ . The other relevant parameters are either determined by already-known binary system parameters of PSR J0023+0923 (Table 1) or the equations in Section 2.2. Besides the Table 1 parameter values, these are  $\mathcal{T} \approx 0.42 \mu\text{s}$ ,  $\nu \approx 24 \text{ rad/d}$ , and  $\theta \approx 1.147$ . If the PSR J0023+0923 system had a Trojan with these properties, the TOA residuals would be of the order of tenths of  $\mu\text{s}$ , consistent with  $\mathcal{T}$ .

We plot this function for an example set of parameters in Figure 3. The timing model, Equation 4, would cause TOA residuals, which are the measured TOAs minus the predicted TOAs, if a Trojan in the system was not accounted for.

While pulsar timing cannot reveal the semi-major axis of the pulsar’s orbit around the system center of mass ( $a_p$ ) directly, it can measure its projection onto the plane of the sky

$$K \equiv \frac{a_p}{c} \sin I. \quad (21)$$

This is useful quantity because it can be related to the masses of the co-orbitals through

$$K = \alpha \sqrt{1 - \delta(1 - \delta)} \quad (22)$$

by setting  $K$  to be the amplitude of the two-body degenerate term of the three-body system (see Appendix A). The value of  $K$  is known quantity for any timed binary pulsar *a priori* to any Trojan search.

In a system with an already known  $n_b$  and  $K$ , measuring the four libration parameters— $\mathcal{T}$ ,  $\nu$ ,  $\theta$ , and  $\varphi$ , the additional parameters required to describe Equation 20—can reveal many physical properties of the system. To do so, we solve Equations 17, 22, and 18 ana-

lytically for  $\delta$ ,  $\alpha$ , and  $z$ :

$$\delta = \frac{2\beta}{\sqrt{3} + \beta} \text{ where } \beta = \tan(\theta - \pi/3), \quad (23)$$

$$\alpha = \frac{K}{\sqrt{1 - \delta(1 - \delta)}}, \quad (24)$$

$$z = \frac{\mathcal{T}}{\alpha\delta(1 - \delta)}. \quad (25)$$

Therefore, Equation 23 shows that  $\theta$  gives a direct measure of the relative Trojan mass,  $\delta$ . Upon assuming a pulsar mass, the companion and Trojan masses are

$$m_c = \frac{1 - \kappa}{1 + \kappa} m_p, \quad (26)$$

$$m_T = \frac{\delta}{1 - \delta} m_c. \quad (27)$$

The orbital inclination can be determined too, using the Newtonian binary mass function

$$\frac{f}{M_\odot} = \frac{(m_c \sin I)^3}{(m_p + m_c)^2} = \frac{K^3}{T_\odot} n_b^2, \quad (28)$$

where  $T_\odot = 4.925490947641... \mu\text{s}$  is the nominal solar mass parameter.<sup>42</sup>

### 2.2.1. Determination of Libration Parameters

We adapt the search methodology of L. Dey et al. (2026), originally developed for freely floating interstellar objects (FFOs), to our Trojan search. In order to seek out the libration delays of Equation 20, we model not only  $\Delta\tau$ , but also white noise, red noise, and the ordinary pulsar timing model, which includes parameters such as pulsar spin period, spin period derivatives, sky position, and binary parameters (see R. T. Edwards et al. 2006; J. Luo et al. 2019, 2021; A. Susobhanan et al. 2024 for more-detailed discussions on the ordinary pulsar timing model). We model the noise and timing model in the exact same way as L. Dey et al. (2026). Noise and timing modeling are handled in the ENTERPRISE Python library (J. A. Ellis et al. 2019; A. D. Johnson et al. 2023). We also use the PTMCMCSampler Python library (J. Ellis & R. van Haasteren 2017; A. D. Johnson et al. 2023), which is an implementation of the parallel tempering Markov-Chain Monte Carlo (PTMCMC) method (see, for example, D. J. Earl & M. W. Deem 2005; W. Vousden et al. 2016 for discussions on PTMCMC). Unlike L. Dey et al. (2026), we used sixteen temperature chains rather than just one because

the posterior space in our case can be highly multimodal (see Section 4.3).

We do not have to worry about degeneracies between the noise modeling and the libration frequency. The red noise is modeled as frequencies in integer multiples of  $1/T_{\text{span}}$ , where  $T_{\text{span}}$  is the time span of TOAs for a given pulsar, up to  $30/T_{\text{span}}$ . The highest such frequency for the eight NG15yr pulsars of interest is  $30/(3.4 \text{ yr}) \sim 9 \text{ yr}^{-1}$ . The libration frequencies are of order  $1 \text{ day}^{-1} \sim 400 \text{ yr}^{-1}$  (see Figures 5, 6, and 7). Therefore, the red noise frequency space and the libration frequency space are disjoint.

### 2.2.2. Libration Priors

We adopt uninformative priors on the libration parameters,  $\mathcal{T}$ ,  $\nu$ ,  $\theta$ , and  $\varphi$ . We also adopt the same priors on the red noise as in (L. Dey et al. 2026). We do not search for  $n_b$  in our MCMC approach as the mean motion is already well constrained by the timing model.

- We choose a log-uniform distribution for  $\mathcal{T}$  of  $\log(\mathcal{T}/\text{s}) \sim \mathcal{U}(-12, -4)$ . The lower limit of  $-12$  was chosen because such a signal strength is far beneath the noise floor of NG15yr MSPs, which is on the order of 0.1–1 microseconds (G. Agazie et al. 2023). The  $-4$  upper limit is in place because a signal of such strength would already easily be detected by eye in the TOA residuals.
- Our prior on  $\nu$  is  $\nu \sim \mathcal{U}(\nu_{\text{min}}, \nu_{\text{max}})$ . The maximum real-valued  $\nu$  in Equation 15 is  $n_b/\sqrt{2}$ . Therefore, this is our  $\nu_{\text{max}}$ . The minimum value,  $\nu_{\text{min}}$ , is determined by finding the smallest  $\mu$  for a given binary mass function (Equation 28) and inserting that  $\mu$  into Equation 13. Such a  $\mu$  is found by setting  $\sin I = 1$  and the pulsar mass to the most massive discovered pulsar ( $\sim 2.5 M_\odot$ ; N. Clifford 2019).
- We choose the prior  $\theta \sim \mathcal{U}(\pi/3, 2\pi/3)$  because these bound the physical range of  $\theta$  according to Equation 17, given  $\delta \in [0, 1]$ . We also investigate the  $\theta \sim \mathcal{U}(0, 2\pi)$  prior to account for any nonphysical signals that may enter our physically-motivated prior space due to uncertainties in  $\theta$ . Lastly, we look in  $\log \xi$  space, where  $\theta = \pi/3 + \xi$ , with a  $\log \xi \sim \mathcal{U}(-6.2, \log(\pi/3))$  prior. The minimum of  $-6.2$  is chosen because this gives the corresponding  $\theta$  when the Trojan is 1 lunar mass and the secondary is  $0.05 M_\odot$ , the most massive companion satisfying Equation 1 when  $m_p = 1.35 M_\odot$ . A search in  $\log \xi$ , where

$$\xi = \theta - \pi/3, \quad (29)$$

<sup>42</sup> This is a defined quantity. See Section 3.4.1 of P. C. Freire & N. Wex (2024) for a brief discussion on  $T_\odot$ .

allows us to probe small Trojan masses in the  $L_5$  Lagrange point (Section 4.3). We do not carry out an analogous  $\theta = 2\pi/3 - \xi'$  search over a uniform  $\log \xi'$  prior because none of our positive detections are near  $\theta = 2\pi/3$ .

- We choose the prior  $\varphi \sim \mathcal{U}(0, 2\pi)$  because  $\varphi$  is an arbitrary phase. We take special care to ensure  $\varphi$  is  $2\pi$ -periodic in our use of `PTMCMCSampler`.

### 3. SELECTED PULSARS AND THEIR OBSERVATIONAL DATA

According to the Australia Telescope National Facility Pulsar Catalog (R. N. Manchester et al. 2005),<sup>43</sup> there are 72 pulsar binary systems that satisfy Equation 1 when  $m_T = 0$ ,  $m_p = 1.35 M_\odot$ , and  $m_c$  is determined by the Newtonian mass function (Equation 28) when  $\sin I = 1$ , where  $I$  is the pulsar system’s orbital inclination with respect to the plane of the sky. We define  $m_{c, \min}$  as the minimum secondary mass when  $m_p = 1.35 M_\odot$ . Note that  $m_{c, \min} = m_c$  when  $I = 90^\circ$ . Choosing  $m_T = 0$  in evaluating Equation 1 gives us systems that may have Trojans, provided they are not too massive. Any discovered pulsar Trojans would have non-zero masses that still satisfy Equation 1. Out of these 72 systems, we restrict this study to PSR J1641+8049 and the eight systems that are in the NG15yr dataset (see Table 1) due to their high observation cadence, long timing baseline, and availability of the dataset. Other datasets also satisfy these criteria (e.g., J. Antoniadis et al. 2023; A. Zic et al. 2023), but we leave those analyses for future work due to differences in the noise modeling and observatories. Useful properties of these pulsars can be found in Table 1. For PSR J1641+8049, we use the method developed by E. B. Ford & B. S. Gaudi (2006) to seek out Trojan-caused inconsistencies between the pulsar-companion conjunction times as measured by optical lightcurves of the system (A. Y. Kirichenko et al. 2024) and those predicted by radio pulsar timing (see Section 2.1). For the eight NG15yr pulsars of interest, we adapt the method of A. Leleu et al. (2015) to look for TOA residuals caused by Trojan librations—a method that only requires TOAs (see Section 2.2).

#### 3.1. Optical Data

The first optical observations of the PSR J1641+8049 counterpart were reported by R. S. Lynch et al. (2018), revealing strong brightness variations tied to the binary period. The detection triggered further optical studies:

using the High PERFORMANCE CAMera (HiPERCAM) installed at the 10.4m Gran Telescopio Canarias (GTC), D. Mata Sánchez et al. (2023) performed phase-resolved multi-band photometric observations and analysed the light curves of the system, yielding its binary parameters and the distance. A. Y. Kirichenko et al. (2024) carried out independent phase-resolved multi-band optical studies with the Optical System for Imaging and low Resolution Integrated Spectroscopy (OSIRIS) at the GTC and performed a comparative light-curve analysis using both the HiPERCAM and OSIRIS datasets.

As demonstrated by both studies, the PSR J1641+8049 system light curves show a single-peaked sinusoidal-like modulation per orbital period with a maximum when the side of the companion heated by the neutron star is directed toward the observer (superior conjunction) and a minimum when the cold back side is visible (inferior conjunction). The system parameters obtained by A. Y. Kirichenko et al. (2024) through the light curve analysis, including the distance to the source 4.6–4.8 kpc and the orbital inclination  $56$ – $59^\circ$ , are found to be consistent with those of D. Mata Sánchez et al. (2023). However, the optical flux of the source at the maximum brightness phase faded by a factor of  $\sim 2$  as compared with the values reported in the D. Mata Sánchez et al. (2023) study. Despite this variability, the companion’s irradiated hemisphere remains among the hottest (8000–9500 K) observed in the known black widow systems.

#### 3.2. Radio Pulsar Timing Data

The times of arrival for PSR J1641+8049 came from the CHIME/Pulsar backend (M. Amiri et al. 2021) on the Canadian Hydrogen Intensity Mapping Experiment (CHIME) radio telescope (M. Amiri et al. 2022). These were used in calculating the times of superior conjunction.

Of the eight selected NG15yr pulsars, four were observed with the Arecibo Observatory (AO; PSRs J0023+0923, J1745+1017, J2214+3000, and J2234+0944) and four with the Green Bank Telescope (GBT; PSRs J0610–2100, J0636+5128, J1705–1903, and J1719–1438). The TOAs of our selected pulsars cover time spans ( $T_{\text{span}}$ ) ranging from 3.4 yr (PSR J0610–2100) to 9.0 yr (PSR J0023+0923). The near-random telescope cadences with respect to libration phase (see Equations 12 and 20), combined with the years-long timing baselines, ensure that the TOAs effectively sample all libration phases. Therefore, the Nyquist–Shannon sampling theorem criterion is relaxed, and the libration frequencies that are physically allowed (Section 2.2.2) can be well-constrained. We show the

<sup>43</sup> <https://www.atnf.csiro.au/research/pulsar/psrcat>

**Table 1.** Relevant parameters of the binary pulsars in this study. Parentheses give  $1\sigma$  uncertainties on the trailing digit. The RMS is the root-mean-squared of the pulse TOA residuals. If  $m_p = 1.35 M_\odot$ , then the system can only contain Trojans if  $m_c$  is no higher than  $0.05 M_\odot$ , according to Equation 1. The eight pulsars after PSR J1641+8049 are in the NG15yr dataset. We used TOAs from the Gran Telescopio Canarias (GTC), Canadian Hydrogen Intensity Mapping Experiment (CHIME), Arecibo Observatory (AO), and Green Bank Telescope (GBT).

PSR	$P_b$ (hr)	$K$ (lts)	$e_o$	$T_{\text{span}}$ (yr)	RMS ( $\mu\text{s}$ )	$m_{c,\text{min}}$ ( $M_\odot$ )	Telescope
J1641+8049	2.1809748921(3)	0.0640753(2)	$2.2(4) \times 10^{-5}$	2.8	1.88	0.0404	GTC, CHIME
J0023+0923	3.3311794144(4)	0.03484142(4)	$7(2) \times 10^{-6}$	9.0	6.02	0.0164	AO
J0610–2100	6.864384046(3)	0.0734890(2)	$1.8(8) \times 10^{-5}$	3.4	9.41	0.0214	GBT
J0636+5128	1.5972322096(4)	0.00898636(5)	$1.7(7) \times 10^{-5}$	6.3	6.04	0.0069	GBT
J1705–1903	4.414896263(2)	0.1043598(1)	$3(1) \times 10^{-6}$	3.7	3.07	0.0412	GBT
J1719–1438	2.17695076(2)	0.0018216(4)	$5(2) \times 10^{-4}$	3.4	15.80	0.0011	GBT
J1745+1017	17.52579411(2)	0.0881697(6)	$2(1) \times 10^{-5}$	4.5	14.46	0.0137	AO
J2214+3000	9.999190702(3)	0.0590815(2)	$2.1(6) \times 10^{-5}$	8.4	7.31	0.0133	AO
J2234+0944	10.071840895(2)	0.0684298(1)	$7(3) \times 10^{-6}$	7.1	5.76	0.0154	AO

TOA residual time series for PSRs J0023+0923 and J1705–1903 in Figure 4 as characteristic examples of residual time series. Residuals for the other pulsars can be found in Appendix C of G. Agazie et al. (2023). More details about the NG15yr dataset can be found in G. Agazie et al. (2023).

## 4. RESULTS

### 4.1. PSR J1641+8049 Superior Conjunction Inconsistency Result

Using the optical lightcurves of the PSR J1641+8049 system, we identify two times of superior conjunction corresponding to peak light. These are  $T_{o,s} = \{58640.0974(15), 58640.1883(15)\}$  MJD. Note the binary period is 0.09087395384(1) day. The in-system Romer delay is smaller than the uncertainties, so no correction is needed for  $T_{o,s}$ . The corresponding times of superior conjunction as predicted by radio pulsar timing are  $T_{r,s} = \{58640.09735997(5), 58640.18823392(5)\}$  MJD. Here, we use the  $T_{r,s} = T_{\text{asc}} - P_b/4$  equation and subtracted integer multiples of  $P_b$  so that  $T_{r,s}$  is as close as possible to  $T_{o,s}$ . The results are visually summarized in Figure 1.

We find no statistically significant difference in the TSCs, and constrain  $|\Delta t|$  to be no higher than 190 s (95% confidence). Therefore, through Equation 2,  $|\Delta m_T|$  can no higher than  $8 M_J$  between the triangular Lagrange points. Comparing times of superior conjunction also confirms, within the uncertainties, that the companion of PSR J1641+8049 is being heated symmetrically (see D. Kandel & R. W. Romani 2020; G. Voisin et al. 2020 for discussions on asymmetric black widow companion heating). Combining both a non-zero  $\Delta m$  and asymmetric heating in such a way that their effects

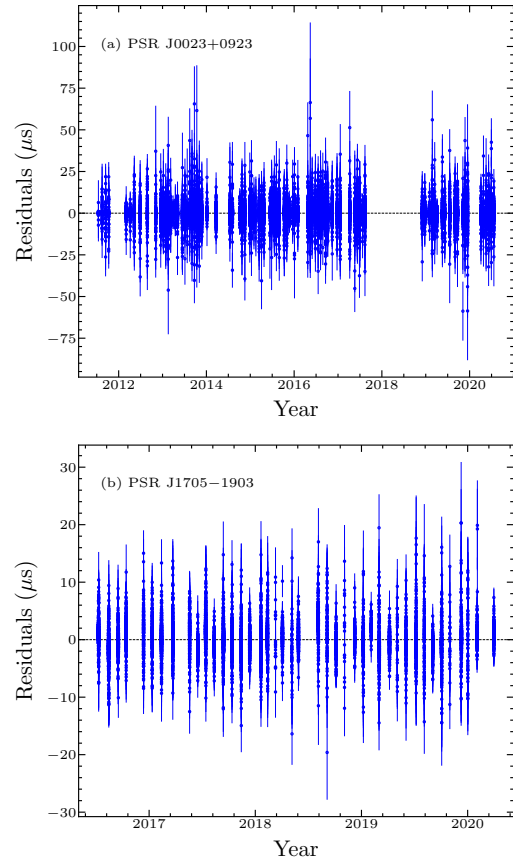


**Figure 4.** The pulse TOA residuals for PSRs J0023+0923 and J1705–1903. The error bars indicate the 68% uncertainty. These are the residuals after the ordinary timing model, but not red noise, has been accounted for (Section 2.2.1). These two pulsars stand out above the others because their TOAs contain minor evidence for the Trojan libration signal (see Section 4.2).

on the time of superior conjunction cancel is also possible.

#### 4.2. Librations Results

With the exceptions of PSRs J0023+0923 and J1705–1903, we find zero evidence of exotrojans in the NG15yr pulsar systems analyzed. In Figure 5 we show a corner plot of the posteriors for PSR J0610–2100, which is characteristic of the other five clear non-detections. To emphasize that these are indeed non-detections, we calculate the Bayes factor,  $\mathcal{B}_{\mathcal{T}}$ , for each NG15yr pulsar. We use the Savage-Dickey formalism (J. M. Dickey 1971) adapted for our model,

$$\mathcal{B}_{\mathcal{T}} = \frac{\text{prior}(\mathcal{T} = 0)}{\text{post}(\mathcal{T} = 0)}, \quad (30)$$

where  $\text{prior}(\mathcal{T} = 0)$  and  $\text{post}(\mathcal{T} = 0)$  are the marginalized prior and posterior probabilities, respectively, when the libration strength is 0 (i.e. Trojans are either entirely absent ( $m_{\mathcal{T}} \equiv 0$ ) or not librating ( $z \equiv 0$ )). Intuitively speaking, this formula describes the relative shift in the probability of a null-detection when TOA data is considered. The libration strength Bayes factor for each NG15yr pulsar is listed in the second column of Table 2.

Upon a positive detection of the signal given by Equation 20, we employ another Bayes factor,

$$\mathcal{B}_{\xi} = \frac{\text{prior}(\theta = \pi/3)}{\text{post}(\theta = \pi/3)}, \quad (31)$$

where  $\text{prior}(\theta = \pi/3)$  and  $\text{post}(\theta = \pi/3)$  are the marginalized prior and posterior probabilities, respectively, when the Trojan mass is zero. Therefore,  $\mathcal{B}_{\mathcal{T}}$  quantifies the support for a positive detection of our Trojan model, while  $\mathcal{B}_{\xi}$  quantifies the support for the detection being from a massive Trojan, rather than a Trojan with a nonphysical mass. We calculate  $\mathcal{B}_{\xi}$  in  $\log \xi$  space rather than  $\theta$  space (hence the subscript) because  $\log \xi$  is more sensitive to low Trojan masses. The non-zero-Trojan-mass Bayes factors are listed in the last column of Table 2 for the two pulsars with positive  $\mathcal{T}$  detections.

Due to mostly non-detections, we place upper limits (ULs) on the libration strength ( $\mathcal{T}_{\text{UL}}$ ) and make additional assumptions on the pulsar and pulsar Trojan populations to map the marginalized posterior on  $\mathcal{T}$  to a Trojan mass UL ( $m_{\mathcal{T},\text{UL}}$ ; see Appendix B for details on the  $\mathcal{T} \mapsto m_{\mathcal{T},\text{UL}}$  mapping). We choose our ULs to represent 95% credibility. Following L. Dey et al. (2026) we put  $\mathcal{T}$  on a linear scale in order to correctly place an upper limit. This requires that we weight the  $\mathcal{T}$  histogram bins by a factor of  $\mathcal{T}$  to account for the Jacobian in converting between the  $\log \mathcal{T}$  and  $\mathcal{T}$  probability distributions. S. Hourihane et al. (2023) show that using a

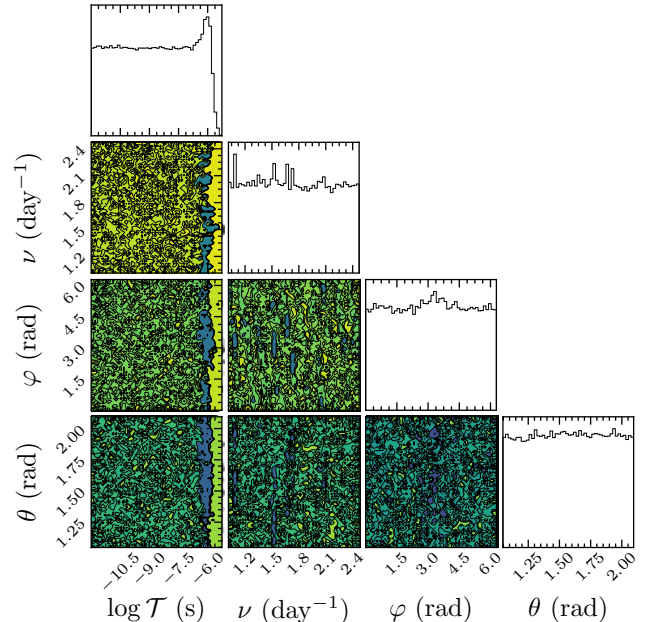


**Figure 5.** The posterior space of the PSR J0610–2100 libration analysis. Each histogram represents the marginalized posterior of the relevant parameter. Each contour plot represents the joint-marginalized posterior of the two relevant parameters. This is a clear non-detection with almost flat posteriors across all parameters. There is a slight preference for  $\log(\mathcal{T}/\text{s}) \sim 10^{-6}$ , which is similar to the noise floor of this pulsar (G. Agazie et al. 2023), though  $\log(\mathcal{T}/\text{s})$  is agnostic to the other three parameters. Furthermore, the Bayes factor for a non-zero  $\log(\mathcal{T}/\text{s})$  is less than 1, so no librations ( $\mathcal{T} \equiv 0$ ) are probabilistically preferred.

PSR	$\mathcal{B}_{\mathcal{T}}$	$\mathcal{T}_{\text{UL}}$ ( $\mu\text{s}$ )	$m_{\mathcal{T},\text{UL}}$ ( $M_{\oplus}$ )	$\mathcal{B}_{\xi}$
J0023+0923	11.5(2)	0.47	0.79	0.95(7)
J0610–2100	0.824(7)	2.8	1.8	-
J0636+5128	0.801(8)	0.37	0.81	-
J1705–1903	5700(300)	1.7	2.7	0.83(5)
J1719–1438	0.73(1)	1.4	2.0	-
J1745+1017	0.792(8)	4.2	1.5	-
J2214+3000	0.90(1)	1.8	1.1	-
J2234+0944	0.96(2)	1.0	0.66	-

**Table 2.** Values of  $\mathcal{T}_{\text{UL}}$ , Bayes factor  $\mathcal{B}_{\mathcal{T}}$  (with 68% uncertainty),  $m_{\mathcal{T},\text{UL}}$ , and  $\mathcal{B}_{\xi}$  for each pulsar. The uncertainty on the Bayes factor is due to the method in calculating the Bayes factor with non-infinite posterior chains. The ULs represent a 95% credibility. Every NG15yr pulsar except PSRs J0023+0923 and J1705–1903 has  $\mathcal{B}_{\mathcal{T}} < 1$ . We do not calculate  $\mathcal{B}_{\xi}$  for these six pulsars. The upper limits placed on PSRs J0023+0923 and J1705–1903 were calculated using the same routine as the other pulsars and are independent of the analysis used in investigating a potential detection in the system in Section 4.3.

linear scale for  $\mathcal{T}$  and weighting in this fashion ensure the upper limits do not depend on the  $\mathcal{T}$  prior lower-bound. We place the values of  $\mathcal{T}_{\text{UL}}$  and  $m_{\text{T}}$  for each pulsar in third and fourth columns, respectively, of Table 2.

Despite positive detections of Equation 20 in the PSR J0023+0923 and J1705–1903 systems, we also place upper limits on them due to the fact that we suspect these are false-positives (see the following subsection). In doing so, we assume the signals are not from true librations, and therefore, we follow the same procedure as for the other pulsars. Thus, the Trojan mass upper limits on these two systems are inconsistent with the Trojan masses as calculated in Table 3 because the upper limits assume a certain distribution in  $z$ , while the results in Table 3 can determine  $z$  from the libration parameters. See Section 4.3 and Appendix B for more details.

#### 4.3. PSRs J0023+0923 and J1705–1903 Libration Results

We find weak evidence of exotrojans in the PSR J0023+0923 and J1705–1903 systems and showcase their posterior corner plots in Figures 6 and 7. For PSR J0023+0923, the posterior space is clearly multimodal, with evidence for sidereal-day-aliasing in  $\nu$ . Aliasing is an observational cadence effect due to the Nyquist-Shannon sampling theorem, where spurious frequencies can fit the data somewhat well in place of the true frequency. In our case, these different frequencies vary from the true frequency by integer multiples of  $f_{\text{sidereal}} \approx 1 \text{ day}^{-1}$ , because the NG15yr TOAs of PSR J0023+0923 were measured by the Arecibo Observatory, a transit instrument. As for all transit instruments, the Arecibo Observatory had limited pointing capabilities and required the sky to rotate over its field of view. Therefore, every TOA of PSR J0023+0923 was observed at roughly the same sidereal time. As mentioned in Section 3.2, the Nyquist-Shannon sampling theorem is weakened by the vast number of observations occurring at different librational phases, which is why one frequency,  $\sim 3.82 \text{ day}^{-1}$ , stands out above the rest. PSR J1705–1903 only shows weak aliasing, because it was observed with the Green Bank Telescope, which has full pointing capabilities. Another feature of both posterior spaces is that  $\theta$  tends towards  $\pi/3$ , which corresponds to  $\delta = 0$ . Therefore, any Trojans in these two systems will be in the  $L_5$  Lagrange point, and thus  $m_c$  and  $m_{\text{T}}$  should be exchanged in Figure 2.

In Figure 8 we show the PSR J0023+0923 posterior space in the  $\pm 0.05\%$  neighborhood of  $\nu = 3.81759 \text{ day}^{-1}$ . We find that the  $\theta$  posterior is fully con-

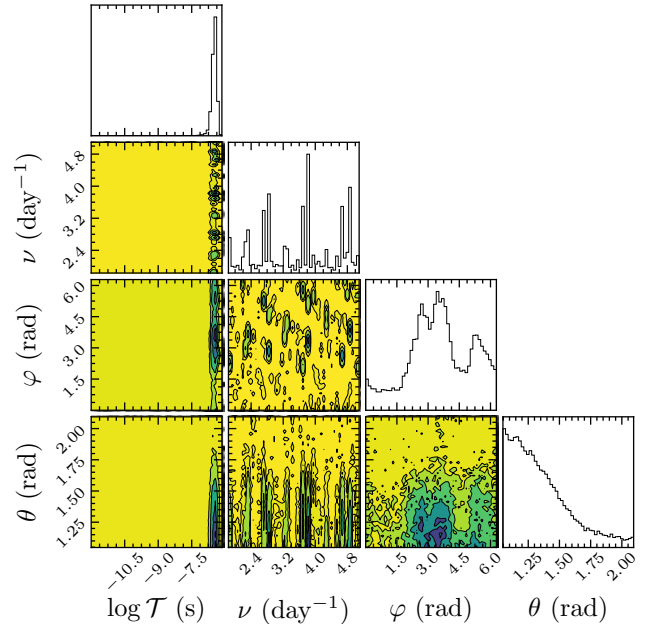


**Figure 6.** The same as Figure 5 except for PSR J0023+0923. With a Bayes factor of 11.5(2), we have a tentative detection of the signal in Equation 20. However, we find that the origin of this signal is unlikely to be caused by a Trojan due to a nonphysical Gaussian-average value for  $\theta$ . See the text for more details.

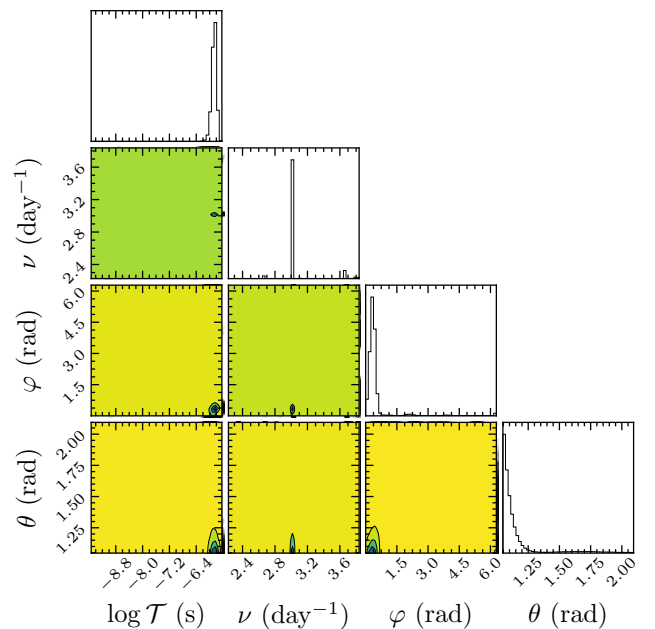


**Figure 7.** The same as Figure 5 except for PSR J1705–1903.

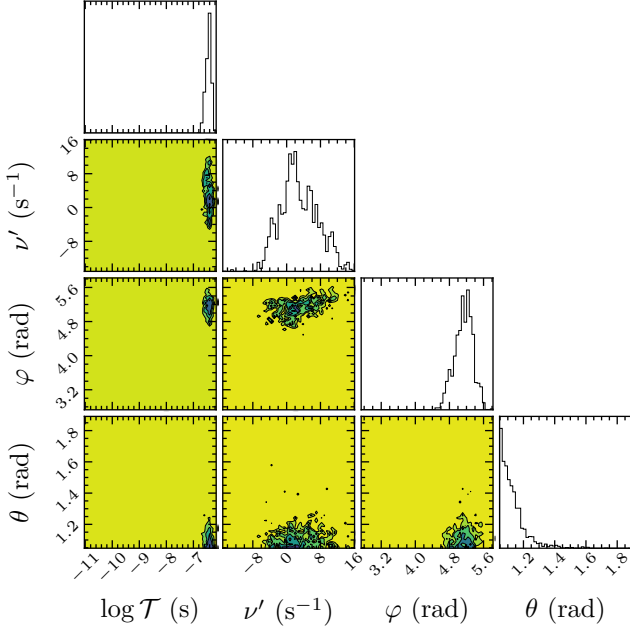


**Figure 8.** The same as Figure 6 (PSR J0023+0923) except the posterior is restricted to the  $\pm 0.05\%$  neighborhood of  $\nu = 3.81759 \text{ day}^{-1}$ . The  $\pm 0.05\%$  width was chosen so that several standard deviations were included. A Fisher information analysis reveals this width to be the expected uncertainty in  $\nu$ . We define  $\nu' = \nu - 3.81759 \text{ day}^{-1}$ . As stated in the text, we find it unlikely that this signal is due to a Trojan.

sistent with that of a Gaussian tail, where the Gaussian is centered at  $\theta \approx 0.64$ , implying  $\delta \approx -0.66$ . Furthermore, we find a Gaussian in  $\theta$  centered at the same value when searching for a Trojan signal when using a  $\theta \sim \mathcal{U}(0, 2\pi)$  prior, rather than the physically valid  $\theta \sim \mathcal{U}(\pi/3, 2\pi/3)$  prior. We included a search over this non-physical prior in order to confirm that the source of the posterior is in the non-physical parameter space. We also search in  $\log \xi$  space (see Section 2.2.2) and find no preferred  $\xi$  (see Figure 9). In fact, we find  $\mathcal{B}_\xi < 1$  for both pulsars. We therefore conclude that the signals associated with the  $\nu \approx 3.82 \text{ day}^{-1}$  and  $3.02 \text{ day}^{-1}$  libration frequencies for PSR J0023+0923 and J1705–1903, respectively, are unlikely to be caused by Trojans (see Section 5 for a discussion on possible other causes). However, for instructive purposes, we carry out the following calculations as if the signals were from a Trojan in each system.

In this paragraph, we only use samples where  $\nu$  is in the  $\pm 0.05\%$  neighborhood of  $\nu = 3.81759 \text{ day}^{-1}$  for PSR J0023+0923 and  $3.01600 \text{ day}^{-1}$  for PSR J1705–1903. Using Equation 23 on the  $\theta$  samples and Equations 15 and 26 on the  $\nu$  samples, we find  $\delta$  and  $q \equiv m_p/m_c$ , placing them in the second and third

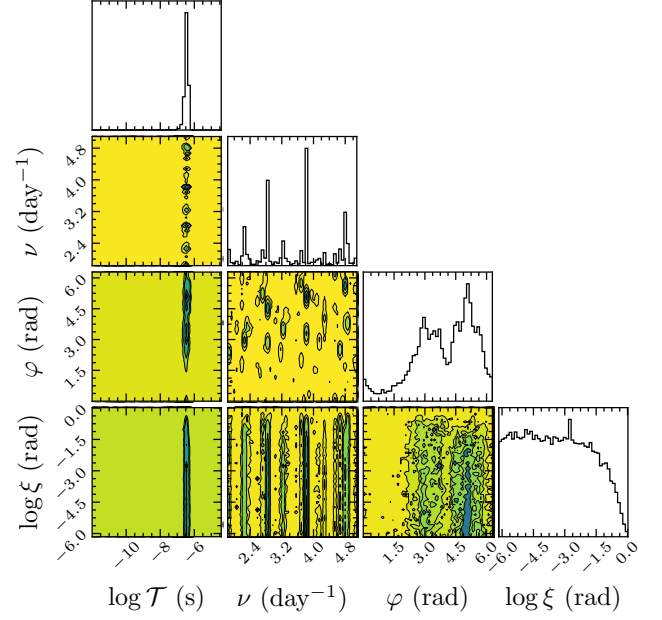


**Figure 9.** The same as Figure 6 (PSR J0023+0923) except  $\log \xi$  is searched over uniformly.

columns, respectively, of Table 3. We then use Equation 25 to calculate  $z$ , which we include in the fourth column of Table 3. Exchanging  $m_c$  and  $m_T$  in the definition of  $\delta$  so that  $m_c$  is the more massive body, and assuming the pulsar mass function of J. Antoniadis et al. (2016) (as in Appendix B), we find  $m_T$ ,  $m_c$ , and  $I$ , placing them in the remaining columns of Table 3. Using an optical light curve analysis of the PSR J0023+0923 system, D. Mata Sánchez et al. (2023) find  $q = 59_{-11}^{+10}$  and  $I = 42_{-3}^{+4}$ . The inconsistency of their measurements with ours is another indication that our detected signal is not from a Trojan.

When we isolate the PSR J0023+0923 posterior space around other peaked libration frequency values, we do find some cases where the marginalized  $\theta$  distribution has Gaussian centers in the physically-acceptable  $\pi/3 \leq \theta \leq 2\pi/3$  interval. While Trojans in the system offer an explanation for these particular libration frequencies, we caution against this conclusion of a Trojan swarm due to the fact that the most-favored  $\nu$  is likely not due to a Trojan.

#### 4.4. Librating Trojan Prevalence

Accepting the conclusion that we found no librating Trojans in the eight inspected systems, we place a 95% upper bound on the prevalence of Trojans that are detectable using the libration method,  $\eta_{T,\text{Lib}}^{\text{UL}}$ . Here, we ignore the clear differences across the systems, such as orbital parameters and available TOAs. While librations become easier to detect with an increasing number

PSR	$\delta$	$q \equiv m_p/m_c$	$z$ (°)	$m_T$ (M <sub>J</sub> )	$m_c$ (M <sub>⊙</sub> )	$I$ (°)
J0023+0923	$0.064^{+0.082}_{-0.049}$	$31.3940^{+0.0004}_{-0.0006}$	$0.0095^{+0.0335}_{-0.0054}$	$3.5^{+5.6}_{-2.7}$	$0.0458^{+0.014}_{-0.002}$	$13^{+1}_{-5}$
J1705–1903	$0.042^{+0.061}_{-0.031}$	$29.6472 \pm 0.0005$	$0.019^{+0.052}_{-0.011}$	$2.4^{+4.0}_{-1.8}$	$0.048^{+0.014}_{-0.002}$	$32^{+3}_{-12}$

**Table 3.** Libration parameters for PSRs J0023+0923 and J1705–1903 if their detected signals are from individual Trojans. Values are derived by exchanging  $m_c$  and  $m_T$  in the definition of  $\delta$  and assuming the pulsar mass function of J. Antoniadis et al. (2016).

of TOAs, our estimate of  $\eta_{T,\text{Lib}}^{\text{UL}}$  is meant as a first-order, approximate constraint.

By Bayes’ Theorem

$$p(\eta_{T,\text{Lib}}|8 \text{ non-detections}) \propto \mathcal{L}(\eta_{T,\text{Lib}}) \cdot p(\eta_{T,\text{Lib}}), \quad (32)$$

where  $p(\eta_{T,\text{Lib}}|8 \text{ non-detections})$  is the probability that  $\eta_{T,\text{Lib}}$  is the true prevalence of librationaly detectable Trojans, given eight systems indeed lacked librationaly detectable Trojans;  $\mathcal{L}(\eta_{T,\text{Lib}})$  is the likelihood of  $\eta_{T,\text{Lib}}$  and is equal to  $p(8 \text{ non-detections}|\eta_{T,\text{Lib}})$ , the probability of eight non-detections given  $\eta_{T,\text{Lib}}$ ; and  $p(\eta_{T,\text{Lib}})$  is the prior probability on  $\eta_{T,\text{Lib}}$ . Choosing a flat prior ( $p(\eta_{T,\text{Lib}}) \propto 1$ ) and noting that  $p(8 \text{ non-detections}|\eta_{T,\text{Lib}}) = (1 - \eta_{T,\text{Lib}})^8$ , we have

$$p(\eta_{T,\text{Lib}}^{\text{UL}}|8 \text{ non-detections}) = \frac{(1 - \eta_{T,\text{Lib}})^8}{\int_0^1 (1 - \eta_{T,\text{Lib}})^8 d\eta_{T,\text{Lib}}}. \quad (33)$$

Therefore, the 95% UL is given by solving

$$\frac{\int_0^{\eta_{T,\text{Lib}}^{\text{UL}}} (1 - \eta_{T,\text{Lib}})^8 d\eta_{T,\text{Lib}}}{\int_0^1 (1 - \eta_{T,\text{Lib}})^8 d\eta_{T,\text{Lib}}} = 0.95 \quad (34)$$

for  $\eta_{T,\text{Lib}}^{\text{UL}}$ . We find  $\eta_{T,\text{Lib}}^{\text{UL}} = 1 - 0.05^{1/9} \approx 28\%$ . This tells us that there is a 95% chance the prevalence of librationaly detectable Trojans is no higher than 28%.

In general, for  $N$  non-detections,  $\eta_{T,\text{Lib}}^{\text{UL}}(N) = 1 - 0.05^{1/(N+1)}$ . We have  $\eta_{T,\text{Lib}}^{\text{UL}}(N) = |\ln(0.05)|/N + \mathcal{O}(1/N^2) \approx 3/N$ . Therefore,  $\eta_{T,\text{Lib}}^{\text{UL}}(N)$  scales like  $1/N$ , so more non-detections constraint  $\eta_{T,\text{Lib}}$  further, but at a decreasing rate.

## 5. DISCUSSION AND CONCLUSIONS

This study presents the first search for pulsar-bound extrojans. Trojans in general are difficult to detect through methods that rely exclusively on the reflex motion of their host star because these effects are degenerate with those of the dominant co-orbital. Therefore, standard pulsar exoplanet searches cannot probe for co-orbital bodies. Trojans instead require explicit searches, due to their unique, subtle effects on the pulse times of arrival. A librating Trojan detection would improve constraints placed on the secondary mass and orbital inclination, giving good motivation for targeted Trojan searches.

We used two distinct methods to place upper mass limits on Trojans in eight pulsar binary systems. One method combines radio pulsar timing with optical-band light curves in order to determine the difference in location between the fictitious combined companion and the actual companion. Upon finding no significant difference, we concluded that the mass difference between the triangular Lagrange points can be no more than 8 M<sub>J</sub> in the PSR J1641+8049 system. Our use of this method reaffirms the symmetry of black widow heating models. The other method requires no optical data but instead relies on the Trojan and secondary librating with respect to their stable configuration. Despite the highly precise pulse times of arrival in the NG15yr narrow-band dataset, we find only weak evidence of librations in only two of the eight NG15yr systems studied here. We place  $\sim 1 M_{\oplus}$  upper limits on the eight NG15yr systems assuming some properties of the pulsar population as well the hypothetical pulsar Trojan population (see Appendix B).

While we find signals consistent with librations in the PSR J0023+0923 and PSR J1703–1903 systems, the signals are likely associated with a nonphysical part of the parameter space whose uncertainties spread into the physically acceptable space. However, if the signals are rather from Trojans, we find  $m_T \sim 2\text{--}4 M_J$ . Other determined properties, like  $m_c$  and  $I$ , of the PSR J0023+0923 system are at odds with D. Mata Sánchez et al. (2023), weakening any conclusion that the detected signal is Trojan-caused. Furthermore,  $\mathcal{B}_{\xi} < 1$  for both pulsar systems, meaning the detections of the Equation 20 timing model are almost certainly false positives with respect to Trojan detection. We suspect that the true origin is due to complex and chaotic mass transfers in black widow systems, due to the fact that PSR J0023+0923 has known orbital variability (A.-S. Bak Nielsen et al. 2020; G. Agazie et al. 2023) and PSR J1703–1903 experiences radio eclipses for roughly 30% of its orbit (G. Agazie et al. 2023). Indeed, the timing of both of these pulsars requires five binary frequency time derivatives ( $dn_b/dt$ ,  $d^2n_b/dt^2$ , ...,  $d^5n_b/dt^5$ ; G. Agazie et al. 2023). We also identify statistically significant red noise in PSR J1703–1903. Additionally, G. Agazie et al. (2023) find that the parallax determination of PSR J0023+0923 is covariant with the binary frequency derivatives, fur-

ther complicating its stable timing. That being said, as to why a model with two frequencies straddling the orbital frequency by the same margin ( $\nu$ ; see Equation A20) is preferred over a simpler type of “noise” is unclear.

In any case, the timing residuals of PSR J0023+0923 possibly favor ( $\mathcal{B}_{\mathcal{T}} = 11.5(2)$ ) Equation 20 being included with the original timing model, and the residuals significantly prefer ( $\mathcal{B}_{\mathcal{T}} = 5700(300)$ ) of the same for PSR J1705–1903. Therefore, the status of these two pulsars in future pulsar timing array datasets may be called into question. Notably, the MeerKAT Pulsar Timing Array has already removed PSR J1705–1903 from its array in its most recent data release (M. T. Miles et al. 2025). While C. Bochenek et al. (2015) show that including up to four orbital frequency derivatives does not affect a pulsar’s sensitivity to gravitational waves, the Trojan libration model has not been applied to any pulsar before this work. If these pulsars are to be included in future pulsar timing array datasets, such as the forthcoming NANOGrav 20-year dataset, more noise modeling or analysis may be required, which may weaken the effectiveness of these pulsars in detecting the gravitational wave background. Conversely, including this new source of “noise” may improve their effectiveness as compared to where the pulsars currently stand.

There are several clear paths to continuing the pulsar Trojan search. There exist myriad light curves of pulsar binary systems, all of which can have their times of superior conjunction compared to those predicted by pulsar timing. Furthermore, if several light curves are obtained on the same pulsar with the explicit goal of lowering the uncertainty in the time of superior conjunction, libration-independent constraints on the pulsar Trojan population will lower in tandem. In terms of the libration method, plenty of TOA data sets are available for analysis, with several high-quality ones in the making. Currently available high-cadence datasets include those from the the European Pulsar Timing Array (J. Antoniadis et al. 2023), the MeerKAT Pulsar Timing Array (M. T. Miles et al. 2025), and the Parkes Pulsar Timing Array (A. Zic et al. 2023). Gamma-ray pulsar timing arrays (e.g., F.-L. Collaboration\*† 2022; M. Kerr et al. 2024) present yet another way to search for Trojan librations. Because this work was done on the NG15yr dataset, the NANOGrav 20-year dataset will allow for the quickest updates on the Trojan mass constraints or may even reveal a detection.

Our analysis reveals that pulsar Trojans detectable through their librations are likely somewhat rare, with there being no more than one for every three pulsars

that satisfy Equation 1. One explanation is that pulsar Trojans are strongly damped into their stable configuration point, lowering the libration amplitude. This seems plausible since pulsar Trojans would have to form from a dense debris or accretion disk. Alternatively, noting that  $\mathcal{T} \propto z \cdot m_{\text{T}}$ , the pulsar Trojan masses may simply be too low to detect for their given distribution in libration amplitude. Another explanation is that the conditions amenable to Trojan formation are also poor environs for those same Trojans. Mass transfer and disk dynamics in pulsar binary systems are clearly turbulent, and so any interloping Trojan may find itself ejected from the system or torn apart. Lastly, conditions in pulsar binaries may never be friendly to Trojan formation to begin with. Future pulsar Trojan searches, as discussed above, will aid in lowering the upper limit on the librating pulsar Trojan prevalence, and will also constrain the non-librating pulsar Trojan occurrence rate through the superior conjunction method.

Our work here not only represents the first search for Trojans in pulsar binary systems, but also, along with L. Dey et al. (2026), showcases a rigorous and thorough way to analyze deterministic signals in pulse TOAs. The search procedure can be extended to ordinary pulsar exoplanets, pulsar exomoons (or, equivalently, in terms of TOA residuals, planets in the S-type orbital configuration), and even massive bodies in our own Solar System. Such a Solar System body would be correlated across all pulsars, because the location of the Solar System barycenter would shift unexpectedly in time. This is the so-called “Earth term” and can be used to, for example, detect unknown massive Trojans of any of the planets, discover unknown primordial black holes that orbit the sun, or constrain the mass of the known objects in the Solar System.

#### DATA AVAILABILITY

The NG15yr narrowband data set is available at <https://zenodo.org/records/14773896> (The NANOGrav Collaboration 2025).

#### AUTHOR CONTRIBUTIONS

J.D.T. led the project, extended the libration theory of A. Leleu et al. (2015) as relevant for black widow systems, produced the figures, conducted the analysis, and prepared the text with input from E.F., L.D., S.Z., A.Y.K., and J.G. L.D. provided the original code infrastructure for the use of ENTERPRISE and PTMCMC before the FFO-to-Trojan transition and offered key insights into the Bayesian inference used. S.Z. and A.Y.K. carried out the optical-band light curve analysis in determining the optical times of superior conjunction and

wrote the corresponding Section 3.1. A.Y.K. provided the optical light curve data and contributed useful discussions regarding PSR J1641+8049. J.G. provided essential high-performance computing support. J.G., P.B.D., M.K., D.J.N., D.L.K., and T.J.W.L. contributed insightful discussions. T.J.W.L. and D.R.L. gave helpful comments. E.F., J.G., P.B.D., M.K., D.J.N., D.L.K., D.R.L., and the remaining authors contributed to the collection and analysis of the NANOGrav 15 yr dataset.

## ACKNOWLEDGMENTS

We thank Reynier Squillace and the anonymous reviewer for helpful comments. Computational resources were provided by the Link HPC cluster and cyber-infrastructure, which is maintained by the Center for Gravitational Waves and Cosmology at West Virginia University and funded in part by NSF IIA-1458952 & NSF PHY-2020265. Additional computational resources were provided by the WVU Research Computing Thorny Flat HPC cluster, partly funded by NSF OAC-1726534. This research was made possible by the NASA West Virginia Space Grant Consortium, Grant # 80NSSC25M7079, which provided individual support to J.D.T. This work has been carried out as part of the NANOGrav collaboration, which receives support from the National Science Foundation (NSF) Physics Frontiers Center award numbers 1430284 and 2020265. The Arecibo Observatory is a facility of the NSF operated under a cooperative agreement (No. AST-1744119) by the University of Central Florida (UCF) in alliance with Universidad Ana G. Méndez (UAGM) and Yang Enterprises (YEI), Inc. The Green Bank Observatory is a facility of the NSF operated under a cooperative agreement by Associated Universities, Inc. The National Radio Astronomy Observatory is a facility of the NSF operated under a cooperative agreement by Associated Universities, Inc. P.R.B. is supported by the Science and Technology Facilities Council, grant number ST/W000946/1. P.R.B. is supported by the Sci-

ence and Technology Facilities Council, grant number ST/W000946/1. H.T.C. acknowledges funding from the U.S. Naval Research Laboratory. Pulsar research at UBC is supported by an NSERC Discovery Grant and by CIFAR. K.C. is supported by a UBC Four Year Fellowship (6456). M.E.D. acknowledges support from the Naval Research Laboratory by NASA under contract S-15633Y. T.D. and M.T.L. received support by an NSF Astronomy and Astrophysics Grant (AAG) award number 2009468 during this work. E.C.F. is supported by NASA under award number 80GSFC24M0006. D.C.G. is supported by NSF Astronomy and Astrophysics Grant (AAG) award #2406919. D.R.L. and M.A.M. are supported by NSF #1458952. M.A.M. is supported by NSF #2009425. The Dunlap Institute is funded by an endowment established by the David Dunlap family and the University of Toronto. T.T.P. acknowledges support from the Extragalactic Astrophysics Research Group at Eötvös Loránd University, funded by the Eötvös Loránd Research Network (ELKH), which was used during the development of this research. H.A.R. is supported by NSF Partnerships for Research and Education in Physics (PREP) award No. 2216793. S.M.R. and I.H.S. are CIFAR Fellows. Portions of this work performed at NRL were supported by ONR 6.1 basic research funding. S.Z. and A.K. thank Daniel Mata Sanchez for providing the optical data. SZ acknowledges the DGAPA-PAPIIT grant IN119323. AK acknowledges the DGAPA-PAPIIT grant IA105024.

*Facilities:* GTC, CHIME, GBT, Arecibo

*Software:* PINT (J. Luo et al. 2019, 2021), rebound (H. Rein & S. F. Liu 2012; H. Rein & D. S. Spiegel 2015), ENTERPRISE (J. A. Ellis et al. 2019; A. D. Johnson et al. 2023), enterprise\_extensions (S. R. Taylor et al. 2021; A. D. Johnson et al. 2023), PTMCMCSampler (J. Ellis & R. van Haasteren 2017; A. D. Johnson et al. 2023), numpy (C. R. Harris et al. 2020), matplotlib (J. D. Hunter 2007), corner (D. Foreman-Mackey 2016).

## APPENDIX

### A. EFFECT OF LIBRATIONS ON PULSAR TIMES OF ARRIVAL

Here, we largely follow the calculations of A. Leleu et al. (2015) except we include the  $\mathcal{O}(\nu/n_b)$  term that cannot be ignored for the pulsar companion masses of interest in our search. Many of the variables are defined in Section 2.2, but we do repeat some details here for clarity. Referencing Figure 2, we have the Trojan and

companion librating with respect to each other, with the libration angle given by  $\zeta = z \cos(\nu \tilde{t} + \varphi) + \pi/3$  (Equation 12). The mass-averaged longitude,  $\lambda = n_b \tilde{t} + \lambda_0$ , follows the mean motion and is unaffected by the librations. The angles of the Trojan and companion with respect to  $\lambda$  are  $\delta\zeta$  and  $(1-\delta)\zeta$ , respectively. Therefore,

as [P. Robutel et al. \(2011\)](#) showed,

$$\lambda_{\text{T}} = \lambda + \delta\zeta, \quad (\text{A1})$$

$$\lambda_{\text{c}} = \lambda - (1 - \delta)\zeta. \quad (\text{A2})$$

The semi-major axes of the Trojan and the companion in the pulsar-centric reference frame also oscillate with respect to the mass-averaged semi-major axis,  $a$ , and are given by [P. Robutel et al. \(2011\)](#) as

$$a_{\text{T}} \approx a \left( 1 - \frac{2\delta\dot{\zeta}}{3n_{\text{b}}} \right), \quad (\text{A3})$$

$$a_{\text{c}} \approx a \left( 1 + \frac{2(1-\delta)\dot{\zeta}}{3n_{\text{b}}} \right). \quad (\text{A4})$$

Explicitly,  $\dot{\zeta} = z\nu \sin(\nu\tilde{t} + \varphi)$ .

In the pulsar-centric reference frame,

$$\mathbf{r}_{\text{T}} = a_{\text{T}} e^{i\delta\zeta} e^{\lambda}, \quad (\text{A5})$$

$$\mathbf{r}_{\text{c}} = a_{\text{c}} e^{i(\delta-1)\zeta} e^{\lambda}, \quad (\text{A6})$$

where we use the  $\mathbf{r} = x + iy$  complex notation. In the barycentric reference frame,

$$\mathbf{r}_{\text{p}} = -\mu[(1-\delta)\mathbf{r}_{\text{T}} + \delta\mathbf{r}_{\text{c}}]. \quad (\text{A7})$$

In the  $z \ll 1$  limit, we find that  $\mathbf{r}_{\text{p}}$  can be separated into two parts,

$$\mathbf{r}_{\text{p}} = -\mathbf{r}_{\text{f}} - \mathbf{r}_{\text{L}}, \quad (\text{A8})$$

where

$$\mathbf{r}_{\text{f}} = \mu a (1 - \delta + \delta e^{-i\pi/3}) e^{i(\lambda + \delta\pi/3)} \quad (\text{A9})$$

is the term that is completely degenerate with that of a single companion and

$$\begin{aligned} \mathbf{r}_{\text{L}} = & \mu a z \delta (1 - \delta) \left( i \cos(\nu\tilde{t} + \varphi) + \frac{2\nu}{3n_{\text{b}}} \sin(\nu\tilde{t} + \varphi) \right) \\ & \times e^{i\pi/3} e^{i(\lambda + \delta\pi/3)} + \mathcal{O}\left(\frac{\nu}{n_{\text{b}}} z^2\right) \end{aligned} \quad (\text{A10})$$

represents non-degenerate terms due to librations. By convention, we place the Earth such that it lies in the  $\hat{x}\hat{z}$ -plane (see [Figure 2](#)) and makes an angle  $I$  with the  $\hat{z}$ -axis. Therefore, by [Equation 4](#),

$$\Delta\tau_{\text{full}} = \Re(\mathbf{r}_{\text{f}} + \mathbf{r}_{\text{L}}) \frac{\sin I}{c}, \quad (\text{A11})$$

where  $\Delta\tau_{\text{full}}$  denotes the full Rømer delay due to the Trojan and companion. The final  $\Delta\tau$  does not include terms degenerate with the timing model.

For the degenerate term, we have

$$\begin{aligned} \Re(\mathbf{r}_{\text{f}}) \frac{\sin I}{c} = & \frac{\mu a \sin I}{c} \sqrt{1 - \delta(1 - \delta)} \\ & \times \cos \left[ n\tilde{t} + \lambda_0 + \delta\frac{\pi}{3} - \arctan \left( \frac{\delta\sqrt{3}}{2 - \delta} \right) \right]. \end{aligned} \quad (\text{A12})$$

This is already included in the timing model ([Section 2.2.1](#)), and so we can exploit the fact that  $T_{\text{asc}}$  and  $K = \alpha\sqrt{1 - \delta(1 - \delta)} = \mu a \sin I \sqrt{1 - \delta(1 - \delta)}/c$  are already known. Without prior knowledge of a Trojan,

$$K_2 = \frac{m_{\text{f}}}{m_{\text{p}} + m_{\text{f}}} \frac{a \sin I}{c}, \quad (\text{A13})$$

where  $K_2$  is the ordinary two-body equivalent to  $K$ . Setting  $K = K_2$  gives the mass of the combined fictitious object,

$$\begin{aligned} m_{\text{f}} = & \frac{m_{\text{p}}(m_{\text{T}} + m_{\text{c}})\sqrt{1 - \delta(1 - \delta)}}{m_{\text{p}} + (m_{\text{T}} + m_{\text{c}})(1 - \sqrt{1 - \delta(1 - \delta)})} \quad (\text{A14}) \\ = & (m_{\text{c}} + m_{\text{T}})\sqrt{1 - \delta(1 - \delta)} + \mathcal{O}\left(\frac{m_{\text{T}}}{m_{\text{p}}}, \frac{m_{\text{c}}}{m_{\text{p}}}\right). \end{aligned}$$

To zeroth order in the orbital eccentricity, [C. Lange et al. \(2001\)](#) defined  $T_{\text{asc}}$  such that  $\Delta\tau_2 = K \sin(\Phi) = K \sin(n_{\text{b}}\tilde{t})$ , where  $\Delta\tau_2$  is the time delay from an ordinary two-body system and  $\Phi = n_{\text{b}}\tilde{t}$ .  $\phi = \Phi - \pi/2$  is shown in [Figure 2](#). The  $-\pi/2$  phase difference arises from how [C. Lange et al. \(2001\)](#) reference  $\Phi$  to the negative  $\hat{y}$ -axis of our convention. Therefore,

$$\phi_0 = -\frac{\pi}{2}. \quad (\text{A15})$$

Matching the phases of  $\Delta\tau_2$  and  $\Re(\mathbf{r}_{\text{f}}) \sin(I)/c$  gives

$$\lambda_0 + \delta\frac{\pi}{3} - \arctan\left(\frac{\delta\sqrt{3}}{2 - \delta}\right) = -\frac{\pi}{2}. \quad (\text{A16})$$

Therefore,  $\phi$  and  $\lambda$  are close but not identical, with

$$\phi - \lambda = \frac{\delta\pi}{3} - \arctan\left(\frac{\delta\sqrt{3}}{2 - \delta}\right) \in \sim [-0.02, 0.02]. \quad (\text{A17})$$

Note that  $\phi \equiv \lambda$  only when  $\delta = 0, 1/2$ , or  $1$ .

Continuing [Equation A11](#) with the non-degenerate term, and ignoring  $\mathcal{O}(\nu z^2/n_{\text{b}})$  effects, we have

$$\begin{aligned} \Re(\mathbf{r}_{\text{T}}) \frac{\sin I}{c} = & \frac{\mu a \sin I}{c} z \delta (1 - \delta) \\ & \times \left[ \cos(\nu\tilde{t} + \varphi) \cos \left( n\tilde{t} + \lambda_0 + \delta\frac{\pi}{3} + \frac{5\pi}{6} \right) \right. \\ & \left. + \frac{2\nu}{3n_{\text{b}}} \sin(\nu\tilde{t} + \varphi) \cos \left( n\tilde{t} + \lambda_0 + \delta\frac{\pi}{3} + \frac{\pi}{3} \right) \right]. \end{aligned} \quad (\text{A18})$$

The overall coefficient defines  $\mathcal{T}$  and the phase

$$\theta = \lambda_0 + \delta\frac{\pi}{3} + \frac{5\pi}{6} \quad (\text{A19})$$

is defined for simplification. Combining [Equations A16](#) and [A19](#) gives [Equation 17](#). The pulsar timing residuals

that are not degenerate with the timing model are given by Equation A18 and simplified in Equation 20.

We can write Equation 20 in a way that shows the periodicity involved directly, and represents how it would appear in the frequency domain. Namely,

$$\Delta\tau = \mathcal{T} \sum_{\pm} \left( \frac{1}{2} \mp \frac{1}{3} \frac{\nu}{n_b} \right) \cos [(n_b \pm \nu)\tilde{t} + (\theta \pm \varphi)], \quad (\text{A20})$$

where  $\sum_{\pm}$  denotes the sum over the plus and minus terms (e.g.,  $\sum_{\pm}(a \pm b) = (a + b) + (a - b)$ ). Thus, in frequency space, we expect to see a double peak around  $n_b$  at  $n_b \pm \nu$ , where the  $n_b - \nu$  peak is stronger. A. Leleu et al. (2015) identify this double peak structure in their Figure 12. We conducted three-body simulations in the integrator REBOUND (H. Rein & S. F. Liu 2012; H. Rein & D. S. Spiegel 2015) and verify that the  $n_b - \nu$  peak is stronger when  $\mathcal{O}(\nu/n_b)$  term cannot be ignored due to  $\mu$  being sufficiently high (see Equation 13).

We identify two corrections to the model in A. Leleu et al. (2015), even after we remove the  $\mathcal{O}(\nu/n_b)$  term. The first correction stems from their Equation 30, line 2. Here, they list  $i(1 - \delta)$ , which instead should be  $i(\delta - 1)$ . This is because in their Equations 9 and 10, there is a minus sign in front of the  $i(1 - \delta)$  exponent. This error leads to an additional factor of  $\sqrt{3}$  in their derivation of  $S_1^* = S_{-1}^*$  (see their Equation 32), which are equivalent to our  $\mathcal{T}/2$ . We place a superscript asterisk (\*) on variables in their notation to avoid confusion.

Another error stems from their Equation 11, and has less obvious effects due to differences in convention. Here, there should be an overall minus sign on the right-hand side of their Equation 11 so that the center of mass is at the origin of the barycentric frame, by definition. This error leads to misattribution of their  $\phi_{\pm 1}^*$ , which are equal to our  $(\theta \pm \varphi)$ . In order to compare our results to theirs, we first map our convention to theirs. The mapping is

$$(\nu T_{\text{asc}} + \varphi, n_b T_{\text{asc}} + \lambda_0) \mapsto (-\nu t_0^*, \lambda_0^*). \quad (\text{A21})$$

Then we obtain

$$\phi_{\pm 1}^* = \theta \pm \varphi = \lambda_0^* + \delta\pi/3 + 5\pi/6 \mp \nu t_0^*. \quad (\text{A22})$$

Their  $\phi_{\pm 1}^*$  has a phase addition of  $-\pi/6$ , rather than  $5\pi/6$ . We note that neither of their errors affects the model waveform, but rather the physical implications (such as assigning masses or the inclination to a system with given libration parameters).

## B. UPPER LIMITS ON THE TROJAN MASS

To turn an UL on  $\mathcal{T}$  into an upper limit on  $m_T$ , some assumptions have to be made about the population of undetected Trojans in the pulsar binary system, as well as the pulsar and its secondary. Here, we only concern ourselves with the most massive of such Trojans. We start with the definition of  $\mathcal{T} = \alpha z \delta (1 - \delta)$ . Defining  $\epsilon = m_T/m_c$  and ignoring  $\mathcal{O}(\epsilon^2)$  terms, we find

$$\alpha = K \left( 1 + \frac{1}{2} \epsilon \right), \quad (\text{B23})$$

$$\delta = 1 - \epsilon. \quad (\text{B24})$$

Therefore,

$$\mathcal{T} = K z \epsilon \implies m_T = \frac{\mathcal{T} m_c}{K z}. \quad (\text{B25})$$

To find the 95% UL on  $m_T$ , we sample  $\mathcal{T}$ ,  $m_c$ ,  $K$ , and  $z$  from their expected distributions in a Monte Carlo fashion.  $\mathcal{T}$  is sampled from the reweighted marginalized posterior (see Section 4.2).  $K$  is fixed to the value of  $a_p \sin I$  determined in the timing model because its uncertainty is extremely low compared to the other parameters in Equation B25. While pulsar Trojans clearly do not share the same evolutionary history as their Jovian brothers, we choose to sample  $z$  from the distribution of Jupiter Trojans with inclinations less than  $10^\circ$  as shown in Figure 3 of F. Marzari et al. (2003).  $m_c$  is sampled indirectly by solving the binary mass function (Equation 28) for each sample of  $m_p$  and  $\sin I$ . We choose the standard  $\cos I \sim \mathcal{U}(0, 1)$ , which assumes a random orientation on the unit sphere of the vector orthogonal to the orbital plane of the pulsar and companion. We choose  $m_p$  from the bimodal pulsar mass function found by J. Antoniadis et al. (2016).

## REFERENCES

- Agazie, G., Alam, M. F., Anumalapudi, A., et al. 2023, ApJL, 951, L9, doi: [10.3847/2041-8213/acda9a](https://doi.org/10.3847/2041-8213/acda9a)
- Amiri, M., Bandura, K., Boyle, P., et al. 2021, ApJS, 255, 5, doi: [10.3847/1538-4365/abfdcb](https://doi.org/10.3847/1538-4365/abfdcb)
- Amiri, M., Bandura, K., Boskovic, A., et al. 2022, ApJS, 261, 29, doi: [10.3847/1538-4365/ac6fd9](https://doi.org/10.3847/1538-4365/ac6fd9)
- Antoniadis, J., Tauris, T. M., Ozel, F., et al. 2016, arXiv preprint arXiv:1605.01665, doi: [10.48550/arXiv.1605.01665](https://doi.org/10.48550/arXiv.1605.01665)
- Antoniadis, J., Babak, S., Nielsen, A.-S. B., et al. 2023, A&A, 678, A48, doi: [10.1051/0004-6361/202346841](https://doi.org/10.1051/0004-6361/202346841)

- Archibald, A. M., Stairs, I. H., Ransom, S. M., et al. 2009, *Science*, 324, 1411, doi: [10.1126/science.1172740](https://doi.org/10.1126/science.1172740)
- Bailes, M., Bates, S. D., Bhalerao, V., et al. 2011, *Science*, 333, 1717, doi: [10.1126/science.1208890](https://doi.org/10.1126/science.1208890)
- Bak Nielsen, A.-S., Janssen, G. H., Shaifullah, G., et al. 2020, *MNRAS*, 494, 2591, doi: [10.1093/mnras/staa874](https://doi.org/10.1093/mnras/staa874)
- Balsalobre-Ruza, O., De Gregorio-Monsalvo, I., Lillo-Box, J., et al. 2023, *A&A*, 675, A172, doi: [10.1051/0004-6361/202346493](https://doi.org/10.1051/0004-6361/202346493)
- Balsalobre-Ruza, O., Lillo-Box, J., Barrado, D., et al. 2024, *A&A*, 689, A53, doi: [10.1051/0004-6361/202450717](https://doi.org/10.1051/0004-6361/202450717)
- Behrens, E. A., Ransom, S. M., Madison, D. R., et al. 2020, *ApJL*, 893, L8, doi: [10.3847/2041-8213/ab8121](https://doi.org/10.3847/2041-8213/ab8121)
- Bochenek, C., Ransom, S., & Demorest, P. 2015, *ApJL*, 813, L4, doi: [10.1088/2041-8205/813/1/L4](https://doi.org/10.1088/2041-8205/813/1/L4)
- Bottke, W. F., Marschall, R., Nesvorný, D., & Vokrouhlický, D. 2023, *SSRv*, 219, 83, doi: [10.1007/s11214-023-01031-4](https://doi.org/10.1007/s11214-023-01031-4)
- Clifford, N. 2019, doi: [10.18130/v3-bfjj-w888](https://doi.org/10.18130/v3-bfjj-w888)
- Collaboration\*†, F.-L. 2022, *Science*, 376, 521, doi: [10.1126/science.abm3231](https://doi.org/10.1126/science.abm3231)
- Cornish, N. J. 2001, <https://map.gsfc.nasa.gov/ContentMedia/lagrange.pdf>
- Cresswell, P., & Nelson, R. P. 2008, *A&A*, 482, 677, doi: [10.1051/0004-6361:20079178](https://doi.org/10.1051/0004-6361:20079178)
- Danby, J. M. A. 1964, *AJ*, 69, 165, doi: [10.1086/109254](https://doi.org/10.1086/109254)
- Dey, L., Jennings, R. J., Taylor, J. D., et al. 2026, *ApJ*, 997, 116, doi: [10.3847/1538-4357/ae279d](https://doi.org/10.3847/1538-4357/ae279d)
- Dickey, J. M. 1971, *The Annals of Mathematical Statistics*, 42, 204, doi: [10.1214/aoms/1177693507](https://doi.org/10.1214/aoms/1177693507)
- Earl, D. J., & Deem, M. W. 2005, *PCCP*, 7, 3910, doi: [10.1039/B509983H](https://doi.org/10.1039/B509983H)
- Edwards, R. T., Hobbs, G., & Manchester, R. 2006, *MNRAS*, 372, 1549, doi: [10.1111/j.1365-2966.2006.10870.x](https://doi.org/10.1111/j.1365-2966.2006.10870.x)
- Ellis, J., & van Haasteren, R. 2017, doi: [10.5281/zenodo.1037579](https://doi.org/10.5281/zenodo.1037579)
- Ellis, J. A., Vallisneri, M., Taylor, S. R., & Baker, P. T. 2019, <https://github.com/nanograv/enterprise>
- Érdi, B., Nagy, I., Sándor, Z., Süli, Á., & Fröhlich, G. 2007, *MNRAS*, 381, 33, doi: [10.1111/j.1365-2966.2007.12228.x](https://doi.org/10.1111/j.1365-2966.2007.12228.x)
- Ford, E. B., & Gaudi, B. S. 2006, *ApJ*, 652, L137, doi: [10.1086/510235](https://doi.org/10.1086/510235)
- Foreman-Mackey, D. 2016, *JOSS*, 1, 24, doi: [10.21105/joss.00024](https://doi.org/10.21105/joss.00024)
- Freire, P. C., & Wex, N. 2024, *LRR*, 27, 5, doi: [10.1007/s41114-024-00051-y](https://doi.org/10.1007/s41114-024-00051-y)
- Gascheau, M. 1843, *Comptes Rendus*, 16, 393
- Ginzburg, S., & Quataert, E. 2020, *MNRAS*, 495, 3656, doi: [10.1093/mnras/staa1304](https://doi.org/10.1093/mnras/staa1304)
- Giuppone, C., Beaugé, C., Michtchenko, T. A., & Ferraz-Mello, S. 2010, *MNRAS*, 407, 390, doi: [10.1111/j.1365-2966.2010.16904.x](https://doi.org/10.1111/j.1365-2966.2010.16904.x)
- Haffert, S., Bohn, A., De Boer, J., et al. 2019, *Nature Astronomy*, 3, 749, doi: [10.1038/s41550-019-0780-5](https://doi.org/10.1038/s41550-019-0780-5)
- Harris, C. R., Millman, K. J., van der Walt, S. J., et al. 2020, *Nature*, 585, 357, doi: [10.1038/s41586-020-2649-2](https://doi.org/10.1038/s41586-020-2649-2)
- Hippke, M., & Angerhausen, D. 2015, *ApJ*, 811, 1, doi: [10.1088/0004-637X/811/1/1](https://doi.org/10.1088/0004-637X/811/1/1)
- Hourihane, S., Meyers, P., Johnson, A., Chatziioannou, K., & Vallisneri, M. 2023, *PhRvD*, 107, 084045, doi: [10.1103/PhysRevD.107.084045](https://doi.org/10.1103/PhysRevD.107.084045)
- Hunter, J. D. 2007, *CSE*, 9, 90, doi: [10.1109/MCSE.2007.55](https://doi.org/10.1109/MCSE.2007.55)
- Janson, M. 2013, *ApJ*, 774, 156, doi: [10.1088/0004-637X/774/2/156](https://doi.org/10.1088/0004-637X/774/2/156)
- Jennings, R. J., Cordes, J. M., & Chatterjee, S. 2020a, *ApJ*, 904, 191, doi: [10.3847/1538-4357/abc178](https://doi.org/10.3847/1538-4357/abc178)
- Jennings, R. J., Cordes, J. M., & Chatterjee, S. 2020b, *ApJ*, 889, 145, doi: [10.3847/1538-4357/ab64df](https://doi.org/10.3847/1538-4357/ab64df)
- Jewitt, D. C., Trujillo, C. A., & Luu, J. X. 2000, *AJ*, 120, 1140, doi: [10.1086/301453](https://doi.org/10.1086/301453)
- Johnson, A. D., Meyers, P. M., Baker, P. T., et al. 2023, *arXiv e-prints*, arXiv:2306.16223, doi: [10.48550/arXiv.2306.16223](https://doi.org/10.48550/arXiv.2306.16223)
- Kandel, D., & Romani, R. W. 2020, *ApJ*, 892, 101, doi: [10.3847/1538-4357/ab7b62](https://doi.org/10.3847/1538-4357/ab7b62)
- Kaplan, M., & Cengiz, S. 2020, *MNRAS*, 496, 4420, doi: [10.1093/mnras/staa1873](https://doi.org/10.1093/mnras/staa1873)
- Keppler, M., Benisty, M., Müller, A., et al. 2018, *A&A*, 617, A44, doi: [10.1051/0004-6361/201832957](https://doi.org/10.1051/0004-6361/201832957)
- Kerr, M., Parthasarathy, A., Cromartie, T., Collaboration, F.-L., et al. 2024, in *38th International Cosmic Ray Conference*, 1595, doi: [10.22323/1.444.1595](https://doi.org/10.22323/1.444.1595)
- Kirichenko, A. Y., Zharikov, S. V., Karpova, A. V., et al. 2024, *MNRAS*, 527, 4563, doi: [10.1093/mnras/stad3391](https://doi.org/10.1093/mnras/stad3391)
- Konacki, M., & Wolszczan, A. 2003, *ApJ*, 591, L147, doi: [10.1086/377093](https://doi.org/10.1086/377093)
- Lange, C., Camilo, F., Wex, N., et al. 2001, *MNRAS*, 326, 274, doi: [10.1046/j.1365-8711.2001.04606.x](https://doi.org/10.1046/j.1365-8711.2001.04606.x)
- Laughlin, G., & Chambers, J. E. 2002, *ApJ*, 124, 592, doi: [10.1086/341173](https://doi.org/10.1086/341173)
- Leleu, A., Robutel, P., & Correia, A. C. M. 2015, *A&A*, 581, A128, doi: [10.1051/0004-6361/201526175](https://doi.org/10.1051/0004-6361/201526175)
- Leleu, A., Robutel, P., Correia, A. C. M., & Lillo-Box, J. 2017, *A&A*, 599, L7, doi: [10.1051/0004-6361/201630073](https://doi.org/10.1051/0004-6361/201630073)
- Li, J., Xia, Z. J., Yoshida, F., Georgakarakos, N., & Li, X. 2023, *A&A*, 669, A68, doi: [10.1051/0004-6361/202244443](https://doi.org/10.1051/0004-6361/202244443)
- Lillo-Box, J., Barrado, D., Figueira, P., et al. 2018a, *A&A*, 609, A96, doi: [10.1051/0004-6361/201730652](https://doi.org/10.1051/0004-6361/201730652)

- Lillo-Box, J., Leleu, A., Parviainen, H., et al. 2018b, *A&A*, 618, A42, doi: [10.1051/0004-6361/201833312](https://doi.org/10.1051/0004-6361/201833312)
- Lin, D., Woosley, S., & Bodenheimer, P. 1991, *Nature*, 353, 827, doi: [10.1038/353827a0](https://doi.org/10.1038/353827a0)
- Luo, J., Ransom, S., Demorest, P., et al. 2019,, *Astrophysics Source Code Library*, record ascl:1902.007
- Luo, J., Ransom, S., Demorest, P., et al. 2021, *ApJ*, 911, 45, doi: [10.3847/1538-4357/abe62f](https://doi.org/10.3847/1538-4357/abe62f)
- Lynch, R. S., Swiggum, J. K., Kondratiev, V. I., et al. 2018, *ApJ*, 859, 93, doi: [10.3847/1538-4357/aabf8a](https://doi.org/10.3847/1538-4357/aabf8a)
- Lyra, W., Johansen, A., Klahr, H., & Piskunov, N. 2009, *A&A*, 493, 1125, doi: [10.1051/0004-6361:200810797](https://doi.org/10.1051/0004-6361:200810797)
- Manchester, R. N., Hobbs, G. B., Teoh, A., & Hobbs, M. 2005, *ApJ*, 129, 1993.  
<https://www.atnf.csiro.au/people/pulsar/psrcat/>
- Marzari, F., Tricarico, P., & Scholl, H. 2003, *Icarus*, 162, 453, doi: [10.1016/S0019-1035\(03\)00026-5](https://doi.org/10.1016/S0019-1035(03)00026-5)
- Mata Sánchez, D., Kennedy, M. R., Clark, C., et al. 2023, *Monthly Notices of the Royal Astronomical Society*, 520, 2217
- Miles, M. T., Shannon, R. M., Reardon, D. J., et al. 2025, *MNRAS*, 536, 1467, doi: [10.1093/mnras/stae2572](https://doi.org/10.1093/mnras/stae2572)
- Moldovan, R., Matthews, J. M., Gladman, B., Bottke, W. F., & Vokrouhlický, D. 2010, *ApJ*, 716, 315, doi: [10.1088/0004-637X/716/1/315](https://doi.org/10.1088/0004-637X/716/1/315)
- Montesinos, M., Garrido-Deutelmoser, J., Olofsson, J., et al. 2020, *A&A*, 642, A224, doi: [10.1051/0004-6361/202038758](https://doi.org/10.1051/0004-6361/202038758)
- Nesvorný, D., Vokrouhlický, D., & Morbidelli, A. 2013, *ApJ*, 768, 45, doi: [10.1088/0004-637X/811/1/1](https://doi.org/10.1088/0004-637X/811/1/1)
- Nițu, I. C., Keith, M. J., Stappers, B. W., Lyne, A. G., & Mickaliger, M. B. 2022, *MNRAS*, 512, 2446, doi: [10.1093/mnras/stac593](https://doi.org/10.1093/mnras/stac593)
- Papitto, A., & Martino, D. d. 2021, in *Millisecond Pulsars* (Springer), 157–200, doi: [10.1007/978-3-030-85198-9\\_6](https://doi.org/10.1007/978-3-030-85198-9_6)
- Patruno, A., & Kama, M. 2017, *A&A*, 608, A147, doi: [10.1051/0004-6361/201731102](https://doi.org/10.1051/0004-6361/201731102)
- Rein, H., & Liu, S. F. 2012, *A&A*, 537, A128, doi: [10.1051/0004-6361/201118085](https://doi.org/10.1051/0004-6361/201118085)
- Rein, H., & Spiegel, D. S. 2015, *MNRAS*, 446, 1424, doi: [10.1093/mnras/stu2164](https://doi.org/10.1093/mnras/stu2164)
- Robutel, P., Rambaux, N., & Castillo-Rogez, J. 2011, *Icarus*, 211, 758, doi: [10.1016/j.icarus.2010.09.014](https://doi.org/10.1016/j.icarus.2010.09.014)
- Shahbaz, T., Linares, M., & Breton, R. 2017, *MNRAS*, 472, 4287, doi: [10.1093/mnras/stx2195](https://doi.org/10.1093/mnras/stx2195)
- Shannon, R., Cordes, J., Metcalfe, T., et al. 2013, *ApJ*, 766, 5, doi: [10.1088/0004-637X/766/1/5](https://doi.org/10.1088/0004-637X/766/1/5)
- Spiewak, R., Bailes, M., Barr, E., et al. 2018, *MNRAS*, 475, 469, doi: [10.1093/mnras/stx3157](https://doi.org/10.1093/mnras/stx3157)
- Susobhanan, A., Kaplan, D. L., Archibald, A. M., et al. 2024, *ApJ*, 971, 150, doi: [10.3847/1538-4357/ad59f7](https://doi.org/10.3847/1538-4357/ad59f7)
- Taylor, J., Ransom, S., & Padmanabh, P. V. 2024, *ApJ*, 964, 128, doi: [10.3847/1538-4357/ad1ce9](https://doi.org/10.3847/1538-4357/ad1ce9)
- Taylor, S. R., Baker, P. T., Hazboun, J. S., Simon, J., & Vigeland, S. J. 2021,  
[https://github.com/nanograv/enterprise\\_extensions](https://github.com/nanograv/enterprise_extensions)
- The NANOGrav Collaboration. 2025,, 2.0.1 Zenodo, doi: [10.5281/zenodo.14773896](https://doi.org/10.5281/zenodo.14773896)
- Voisin, G., Kennedy, M., Breton, R., Clark, C., & Mata-Sánchez, D. 2020, *MNRAS*, 499, 1758, doi: [10.1093/mnras/staa2876](https://doi.org/10.1093/mnras/staa2876)
- Vousden, W., Farr, W. M., & Mandel, I. 2016, *MNRAS*, 455, 1919, doi: [10.1093/mnras/stv2422](https://doi.org/10.1093/mnras/stv2422)
- Wolszczan, A., & Frail, D. A. 1992, *Nature*, 355, 145, doi: [10.1038/355145a0](https://doi.org/10.1038/355145a0)
- Xu, K., Yang, H.-R., Jiang, L., et al. 2024, *ApJ*, 970, 2, doi: [10.3847/1538-4357/ad5319](https://doi.org/10.3847/1538-4357/ad5319)
- Yoshida, F., & Nakamura, T. 2005, *AJ*, 130, 2900, doi: [10.1086/497571](https://doi.org/10.1086/497571)
- Zharikov, S., Kirichenko, A., Zyuzin, D., Shibanov, Y., & Deneva, J. 2019, *MNRAS*, 489, 5547, doi: [10.1093/mnras/stz2475](https://doi.org/10.1093/mnras/stz2475)
- Zharikov, S., Tovmassian, G., Aviles, A., et al. 2013, *A&A*, 549, A77, doi: [10.1051/0004-6361/201220099](https://doi.org/10.1051/0004-6361/201220099)
- Zic, A., Reardon, D. J., Kapur, A., et al. 2023, *PASA*, 40, e049, doi: [10.1017/pasa.2023.36](https://doi.org/10.1017/pasa.2023.36)